MOLECULAR AND CELLULAR BIOLOGY, Apr. 2006, p. 2758–2771 Vol. 26, No. 7
0270-7306/06/$08.00+0 doi:10.1128/MCB.26.7.2758–2771.2006

Overlapping Roles for Homeodomain-Interacting Protein Kinases Hipk1 and Hipk2 in the Mediation of Cell Growth in Response to Morphogenetic and Genotoxic Signals†

Kyoichi Isono,[1] Kazumi Nemoto,[1] Yuanyuan Li,[2] Yuki Takada,[1] Rie Suzuki,[1] Motoya Katsuki,[3] Akira Nakagawara,[2] and Haruhiko Koseki[1]*

RIKEN Research Center for Allergy and Immunology, 1-7-22 Suehiro, Tsurumi-ku, Yokohama 230-0045, Japan[1]; Chiba Cancer Center Research Institute, 666-2 Nitona, Chuoh-ku, Chiba 260-8717, Japan[2]; National Institute for Basic Biology, Okazaki National Research Institute, Okazaki, Japan[3]

Received 5 September 2005/Returned for modification 3 October 2005/Accepted 3 January 2006

Homeodomain-interacting protein kinase 1 (*Hipk1*), 2, and 3 genes encode evolutionarily conserved nuclear serine/threonine kinases, which were originally identified as interacting with homeodomain-containing proteins. Hipks have been repeatedly identified as interactors for a vast range of functional proteins, including not only transcriptional regulators and chromatin modifiers but also cytoplasmic signal transducers, transmembrane proteins, and the E2 component of SUMO ligase. Gain-of-function experiments using cultured cells indicate growth regulatory roles for Hipks on receipt of morphogenetic and genotoxic signals. However, *Hipk1* and *Hipk2* singly deficient mice were grossly normal, and this is expected to be due to a functional redundancy between Hipk1 and Hipk2. Therefore, we addressed the physiological roles of Hipk family proteins by using *Hipk1 Hipk2* double mutants. *Hipk1 Hipk2* double homozygotes are progressively lost between 9.5 and 12.5 days postcoitus and frequently fail to close the anterior neuropore and exhibit exencephaly. This is most likely due to defective proliferation in the neural fold and underlying paraxial mesoderm, particularly in the ventral region, which may be attributed to decreased responsiveness to Sonic hedgehog signals. The present study indicated the overlapping roles for Hipk1 and Hipk2 in mediating cell proliferation and apoptosis in response to morphogenetic and genotoxic signals during mouse development.

Homeodomain-interacting protein kinases (HIPKs) compose an evolutionarily conserved protein family in eukaryotes (37). Based on database screening, it appears that three closely related homologous genes encoding Hipks are conserved in vertebrates, including humans, mice, dogs, cows, and frogs (H. Koseki, unpublished). Mammalian HIPK1, HIPK2, and HIPK3 proteins were originally identified as nuclear protein kinases that function as corepressors for various homeodomain-containing transcriptional regulators, at least in part by forming a complex with Groucho and a histone deacetylase complex (7, 37). There is extensive structural similarity exhibited by the HIPKs with respect to their protein kinase domains, homeoprotein interaction domains, PEST sequences, and C-terminal regions enriched by tyrosine and histidine (YH domains). Although HIPK proteins are mainly found in the nucleus with a novel dot-like subnuclear distribution, which partially overlaps promyelocytic leukemia (PML) nuclear bodies, they are nevertheless also found in the cytoplasm (16, 44, 46). HIPKs have been consistently identified as interactors for a vast range of functional proteins, including not only transcriptional regulators and chromatin modifiers but also cytoplasmic signal transducers, transmembrane proteins, and the E2 component of SUMO ligase (11, 14, 19, 25, 30, 31, 36, 38, 39, 40, 45, 51, 55, 57, 60, 63, 64). These observations suggest that HIPKs have a role in the transcriptional regulation, signal transduction, and regulation of protein stability.

Recently, the growth regulatory functions of HIPKs have been intensively investigated. HIPK1 and HIPK2 have been shown to phosphorylate and activate p53, resulting in the enhancement of p53-dependent transcription, cell growth regulation, and apoptosis initiation upon genotoxic insult (12, 13, 14, 30, 39, 46, 57). Independent of the p53 pathway, HIPK2 also appears to promote apoptosis upon genotoxic stress by down-regulating the transcriptional corepressor C-terminal binding protein (CtBP) (68, 69). In the cytoplasm, it has been shown that HIPK3 transduces proapoptotic signals by death receptors through interaction with TRADD and FADD (55). In particular, HIPK1 appears to be a novel signal transducer in tumor necrosis factor alpha-induced apoptosis signaling, activating the apoptosis signal regulating kinase 1/c-Jun N-terminal kinase/p38 mitogen-activated protein kinase signaling cascade (40). A proapoptotic function of HIPK2 has also been proposed in primary neuronal cells (15, 65). Targeted deletion of the *Hipk2* locus leads to a reduction in apoptosis and an increase in the trigeminal ganglion, whereas overexpression of HIPK2 induces apoptosis in cultured sensory neurons. It is, however, intriguing that the results from a study which used *Hipk1*$^{-/-}$ mouse embryonic fibroblasts (MEFs) transformed by *E1A* and *H*-Ras oncogenes suggested antiapoptotic and oncogenic roles for HIPK1 (39). Therefore, taken together, these findings suggest that HIPK proteins are involved in the control of cell growth in response to various extracellular stimuli and that their functions are also affected by intrinsic cellular

* Corresponding author. Mailing address: RIKEN Research Center for Allergy and Immunology, 1-7-22 Suehiro, Tsurumi-ku, Yokohama 230-0045, Japan. Phone: 81-45-503-9689. Fax: 81-45-503-9688. E-mail: koseki@rcai.riken.jp.

† Supplemental material for this article may be found at http://mcb.asm.org/.

issues, such as the cell lineage, developmental stage, genotoxic stress status, and so on.

It has been suggested that HIPK proteins mediate growth regulation in response not only to genotoxic stress and tumor necrosis factor alpha signaling but also to Wnt and transforming growth factor β (TGF-β) signals. HIPK2 is involved in Wnt-1-dependent phosphorylation and subsequent degradation of c-Myb, which may in turn regulate both the proliferation and apoptosis of hematopoietic cells (36). HIPK2 is also capable of forming a multimeric complex with Axin, a common denominator of Wnt signaling, by regulating the cellular level of β-catenin and p53 (57). Similarly, HIPK2 appears to be required for the inhibition of bone morphogenetic protein (BMP)-induced transcriptional activation by forming a complex with c-Ski and Smad1/4 and regulates TGF-β-induced Jun N-terminal kinase activation and apoptosis (26, 31). Taking these results together, it has been hypothesized that HIPKs recognize multiple cellular inputs for the regulation of cell proliferation and apoptosis by regulating the activity of their interacting proteins and subsequently the transcription of the various target genes. Since Wnt and TGF-β family proteins are essential signaling molecules for the development of various organs, it could be expected that HIPK proteins might play a decisive role during embryogenesis by regulating various morphogenetic signal transductions.

The physiological roles of HIPK family proteins have been addressed by generating mutant alleles for *Hipk1* and *Hipk2* genes. Unexpectedly, however, *Hipk1* and *Hipk2* singly deficient mice were grossly normal and fertile (39, 65). Because of structural and functional similarity between HIPK1 and HIPK2, we hypothesized that single-mutant phenotypes for *Hipk1* and *Hipk2* deficiencies may represent some of the functions of HIPK family proteins based on mutually compensative properties. To address this possibility, we have generated *Hipk1 Hipk2* double mutants by crossing newly generated mutant alleles for both genes and have examined doubly deficient phenotypes. *Hipk1*$^{-/-}$ *Hipk2*$^{-/-}$ double-mutant embryos are progressively lost between 9.5 and 12.5 days postcoitus (dpc), whereas single mutants survive birth. By using compound mutants, we show that Hipk1 and Hipk2 act in synergy to mediate growth regulation upon genotoxic and morphogenetic signals. Hipks may be involved in the integration of various extracellular stimuli and the mediation of appropriate cellular responses during embryogenesis.

MATERIALS AND METHODS

Histological and skeletal analyses. RNA in situ hybridization, terminal deoxynucleotidyltransferase-mediated dUTP-biotin nick end labeling (TUNEL) with an in situ cell death detection kit (AP; Roche), bromodeoxyuridine (BrdU) incorporation analysis, and skeletal preparations were all performed as described previously (23).

Antibodies to mouse Hipk1 and Hipk2. To generate mouse Hipk1- and Hipk2-specific monoclonal antibodies, glutathione *S*-transferase (GST)–Hipk1 (amino acids 702 to 925) and GST-Hipk2 (amino acids 898 to 1051) fusions were purified and injected into BALB/c mice. Consequently, three and five independent hybridoma clones, H1-1, 3H5, and 3G6 against Hipk1 and 1F11, 2D1, 3F7, 3C5, and 3E9 against Hipk2, respectively, were obtained. The H1-1 clone was used for immunostaining while the 2D1 and 3E9 clones were used for immunostaining, immunoblotting, and immunoprecipitation (IP). In addition to the monoclonal antibodies, a rabbit polyclonal antibody against the GST-Hipk2 fusion (T. K. Craft, Japan) was produced.

Immunostaining. Mouse *Hipk1* and *Hipk2* full-length cDNAs were isolated by reverse transcriptase (RT)-PCR with mouse embryonic RNA. Myc-tagged *Hipk1* and *Hipk2* were subcloned into the expression vector pCXN2 (a gift from H. Niwa) at the EcoRI site. These constructs were used for transfection into U2-OS cells with Lipofectamine 2000 (Invitrogen). After 24 h, cells were fixed in 4% paraformaldehyde for 5 min, permeabilized in 0.4% Triton X for 5 min, and subjected to immunofluorescent staining with anti-Myc (9E10) antibody or the anti-Hipk2 or PML (H-238; Santa Cruz Biotechnology) rabbit polyclonal antibody and then visualized by LSM510 confocal microscope (Carl Zeiss). To address subcellular localization of endogenous Hipk1 and Hipk2, MEFs were double-stained with H1-1 and the Hipk2 polyclonal antibody or 2D1 and the anti-PML antibody. The visualization was carried out with an imaging system consisting of an inverted IX71 microscope with UPlanSApo (magnification, 100×; numerical aperture, 1.40; oil; Olympus), a high-speed spinning disk confocal unit equipped with an ArKr laser system (CSU10; Yokogawa Electric Corp., Japan), and a charge-coupled-device camera (ORCA-AG; Hamamatsu Photonics).

Generation of *Hipk1*$^{-/-}$ *Hipk2*$^{-/-}$ mice. Approximately 16.5-kb and 17.5-kb genomic clones for *Hipk1* and *Hipk2*, respectively, were obtained from a λFIX phage library of 129SVJ mice. Each genomic structure was determined by restriction mapping, Southern blotting, and sequencing. The *Hipk1*-targeting vector had the 5′ arm of the XhoI-BamHI fragment (5 kb) from the genomic clone and the 3′ arm of the PCR fragment lacking the initiation codon (1.4 kb) inserted by the *neo* cassette from pHR68 (a gift from T. Kondo) and the *tk* cassette flanked by the 5′ arm. The *Hipk2*-targeting vector had the 5′ arm of the BamHI fragment (3 kb) and the 3′ arm of the BamHI-EcoRI fragment (2.2 kb) from the genomic clone inserted by the *neo* cassette from pMC1-*neo* poly(A) and the *tk* cassette. Germ line chimeras were made with these vectors as described previously (1). Targeted heterozygous mice were backcrossed onto C57BL/6 mice more than three times and intercrossed to obtain homozygous mice. In addition, *Hipk1 Hipk2* double mutants were generated by crossing between *Hipk1* and *Hipk2* single mutants, and *Hipk1*$^{-/-}$ *Hipk2*$^{-/-}$ males and females were mainly maintained for embryological analyses. *Hipk1 Hipk2* double mutants were crossed with *p53* mutant mice (24) to generate *p53 Hipk1 Hipk2* triple mutants.

Immunoprecipitation. Whole-cell extracts were prepared by sonicating an 11.5 dpc embryo in 400 μl of IP buffer (20 mM HEPES [pH 7.8], 10% [vol/vol] glycerol, 150 mM KCl, 0.2 mM EDTA, 1 mM dithiothreitol) containing 4 mM Pefabloc SC (Roche). Lysates were precleared with 50 μl of 50% (vol/vol) protein G-Sepharose at 4°C for 60 min and then incubated for 90 min with *Hipk2* antibody (2D1)-bound protein G, which had already been prepared by mixing 100 μl of the 2D1 culture supernatant with 20 μl of 50% (vol/vol) protein G-Sepharose and 300 μl IP buffer for 90 min. After this 90-min incubation period, protein-bound protein G was washed five times with 800 μl IP buffer, boiled in sodium dodecyl sulfate-sample buffer, separated on 6.5% denaturing polyacrylamide gels, and then analyzed by Western blotting using the Hipk2 antibody (2D1).

Cell culture. MEFs were prepared from 12.5 dpc mouse embryos (33), which were genotyped with yolk sac DNAs and then stored at −80°C. The MEFs were grown in Dulbecco's minimal essential medium supplemented with 10% fetal calf serum and 1% (wt/vol) penicillin/streptomycin on 6-cm dishes at 37°C under 7% CO_2. At passage 4, the culture medium was removed and cells were irradiated with UV (15 or 50 J/m^2) with UV cross-linker (UV Products, Cambridge, United Kingdom) and then recultured in the same medium. Subsequently, at the indicated periods, cells were collected and the trypan blue-stained dead cells and unstained living cells were counted. In addition, these cells were sonicated, and each lysate (30 μg) was subjected to Western blot analysis with anti-p53 (M-19), anti-Bax (B-9), and anti-p21 (F-5) from Santa Cruz Biotechnology, anti-cleaved caspase 3 from Cell Signaling Technology, and anti-CtBP-1 from Upstate. Alternatively, cells on coverslips 12 h after UV (15 and 50 J/m^2) exposure were subjected to a TUNEL assay with the kit described above and then counterstained with eosin.

Luciferase reporter assay. Human lung carcinoma H1299 cells (p53$^{-/-}$) were grown in RPMI 1640 medium supplemented with 10% fetal calf serum and antibiotics and transfected with the Lipofectamine Plus transfection kit (Invitrogen, Grand Island, NY) according to the manufacturer's protocol. Briefly, H1299 cells were seeded at a density of 5×10^4 cells/well in a 12-well tissue culture dish and then cotransfected with 100 ng of p53-responsive luciferase reporter constructs carrying *Bax* and *p21*^{WAF1} promoter, 10 ng of pRL-TK (Promega), and 25 ng of the human or mouse p53 expression plasmid in either the presence or absence of increasing amounts of the pCXN2-Myc-Hipk1 or -Hipk2 construct as described previously (64). The total amounts of DNA used in each transfection were kept constant (510 ng/transfection) using pcDNA3. Luciferase assays were performed 48 h posttransfection with a dual luciferase reporter assay system

(Promega) according to the manufacturer's instructions. To examine the degree of transactivation by DNA damage, transfected cells were exposed to UV (15 and 50 J/m^2) at 24 h posttransfection or treated with cisplatin (Sigma Chemical Co., St. Louis, MO) at a final concentration of 20 μM for 24 h.

Explant culture of presomitic mesoderm and RT-PCR. Strips of the anterior half of the unsegmented paraxial mesoderm were isolated from 9.5 dpc mouse embryos by a combination of dispase treatment and subsequent surgical dissection using a tungsten needle, essentially following a previously described method (21). Mouse tissues were embedded in collagen gels and cultured as described previously (21). Bacterially expressed recombinant Shh protein was added to the culture to a concentration of 100 ng/ml. After 2 days of culture, total RNA was extracted from the explants in collagen gels as described previously (21). Each sample was reverse transcribed by reaction with oligo(dT) primers in a volume of 20 μl. The product of this reaction was serially diluted in a ratio of 3:1, and eventually amounts equivalent to 3, 1, 0.33, 0.11, 0.037, 0.012, 0.0041, and 0.00147 μl of the original reaction volume were subjected to PCR for *Pax1*, *Twist*, and *Hprt* (21). The amounts of total cDNA were corrected by comparing the *Hprt* signal intensities.

RESULTS

The expression of *Hipk* genes during embryogenesis. A prerequisite of the hypothesis that Hipk1 and Hipk2 act in a redundant and mutually compensable manner is the coexpression and colocalization of Hipk family proteins. We therefore compared the expressions of *Hipk* genes during embryogenesis, particularly around 9.5 dpc, at which embryonic stage various inductions that are required for subsequent organ development take place. The expression of *Hipk1* is seen ubiquitously through 8.5 to 10.5 dpc but is slightly enhanced in the neural tube at 10.5 dpc (16; K. Isono, unpublished). *Hipk2* was intensely expressed in the neural tissues, including optic and otic vesicles and newly generated paraxial mesoderm, while other tissues also expressed lower but nevertheless significant amounts of *Hipk2* at 9.5 dpc (Fig. 1A, B, and G) (52). The section at the level of the midbrain revealed the expression in this region and in the emerging and migrating neural crest cells and branchial arches and membranes (Fig. 1C, D, and E). Interestingly, the expression was more intense in the neural crest-derived cells localizing in the vicinity of the surface ectoderm. In the otic vesicle, intense expression was also seen at the region juxtaposed to the surface ectoderm (Fig. 1F). In the prospective trunk region, *Hipk2* expression in the neural tube was slightly more intense in the dorsal than the ventral region and was not seen in the floor plate or the notochord (Fig. 1H). *Hipk2* expression in the paraxial mesoderm was transiently increased in the cranial part of the presomitic mesoderm and newly segmented somites (Fig. 1J). After de-epithelization of the somites, the expression was lower in the sclerotome than in the dermomyotome and was not seen in the myotome (Fig. 1I and J). Therefore, *Hipk2* is expressed in most tissues except for the notochord, floor plate, and myotome. In contrast, *Hipk3* was exclusively expressed in the myocardial wall of the heart primordium and myotome (Fig. 1K, L, and M). These observations indicate that there is coexpression of *Hipk1* and *Hipk2* in various embryonic tissues.

Coexpression and colocalization of Hipk1 and Hipk2 gene products. We went on to examine whether endogenous Hipk1 and Hipk2 proteins were coexpressed in embryonic cells by immunofluorescence. Primary MEFs derived from 12.5 dpc fetuses were used. In all MEFs examined, both proteins were expressed and exhibited punctate localization throughout the nucleus apart from the nucleoles (Fig. 1N, left). Higher magnification views revealed that Hipk1 and Hipk2 were condensed to numerous speckles, which were surrounded by less-condensed foggy domains (Fig. 1N, middle). Condensed speckles for Hipk1 and Hipk2 were mostly separated, and overlapping regions were consequently limited. We also observed their punctate distributions in cytoplasm. Minor fractions of Hipk1 and Hipk2 were contained in PML nuclear bodies as observed in various cell lines (Fig. 1N, right) (K. Isono, unpublished). Therefore, Hipk1 and Hipk2 were coexpressed in primary MEFs. Inclusion to similar extents of both Hipk1 and Hipk2 in PML nuclear bodies may partly indicate their functional similarity.

We next examined the colocalization of Hipk1 and Hipk2 following overexpression, since transiently expressed Hipk1 and Hipk2 in cultured cells were known to localize to subnuclear speckles, which were much larger in size than those seen in MEFs (14, 16, 30, 37, 44). We examined the subnuclear localization of Hipk1 and Hipk2 in U2-OS cells that had been transfected by expression vectors for Myc-tagged Hipk1 and wild-type Hipk2, and these proteins were detected by immunofluorescence with anti-Myc and -Hipk2 antibodies. Under this condition, Hipk1 and Hipk2 strongly colocalized to subnuclear speckles (Fig. 1O). Hipk1 also exhibited a partial colocalization with PML nuclear bodies as well as Hipk2 (Fig. 1P) (14, 16, 30). This may imply that Hipk1 and Hipk2 are potentially capable to colocalize to subnuclear domains in certain cellular contexts, which again indicates their functional similarity.

Generation of *Hipk1 Hipk2* doubly deficient mice. To generate *Hipk1 Hipk2* doubly deficient mice, we independently generated *Hipk1* and *Hipk2* mutant alleles. Since the kinase domains have been shown to be essential for mediating transcriptional repression, the intention was to generate mutant alleles lacking their kinase domains (Fig. 2A and B) (7, 37). The N-terminal halves of the kinase domains of Hipk1 and Hipk2 were encoded by exons containing the start codon. For *Hipk1* mutagenesis, a targeting vector was designed to replace a genomic fragment containing the start codon with a neomycin-resistant (Neo^r) gene cassette (Fig. 2A). For *Hipk2* knockout, a targeting vector was generated to replace the BamHI fragment encoding the C-terminal part of the exon containing the start codon and the flanking intronic region with the Neo^r cassette (Fig. 2B). Both mutations were transmitted into the germ line, and heterozygotes were crossed to generate the homozygotes. Both single homozygous mutant mice were grossly normal and born in a Mendelian ratio as reported for other alleles (39, 65). RT-PCR revealed that both mutations impaired the expression of *Hipk1* and *Hipk2* at least at the regions encoding the kinase domains (Fig. 2C and D). Immunoprecipitation-Western analysis using a monoclonal antibody against the interacting domain of Hipk2 further supported depletion of intact Hipk2 protein in the homozygotic mutants (Fig. 2D). However, we cannot exclude the presence of the C-terminally truncated proteins in both mutants.

Embryonic lethality and exencephaly in *Hipk1 Hipk2* double homozygotes. To explore the phenotypes of *Hipk1*$^{-/-}$ *Hipk2*$^{-/-}$ mice, double heterozygous mice which were viable and fertile were crossed, and naturally delivered newborn pups were genotyped. We found that all of the double homozygotes and about half of the *Hipk1*$^{+/-}$ *Hipk2*$^{-/-}$ embryos were lost during

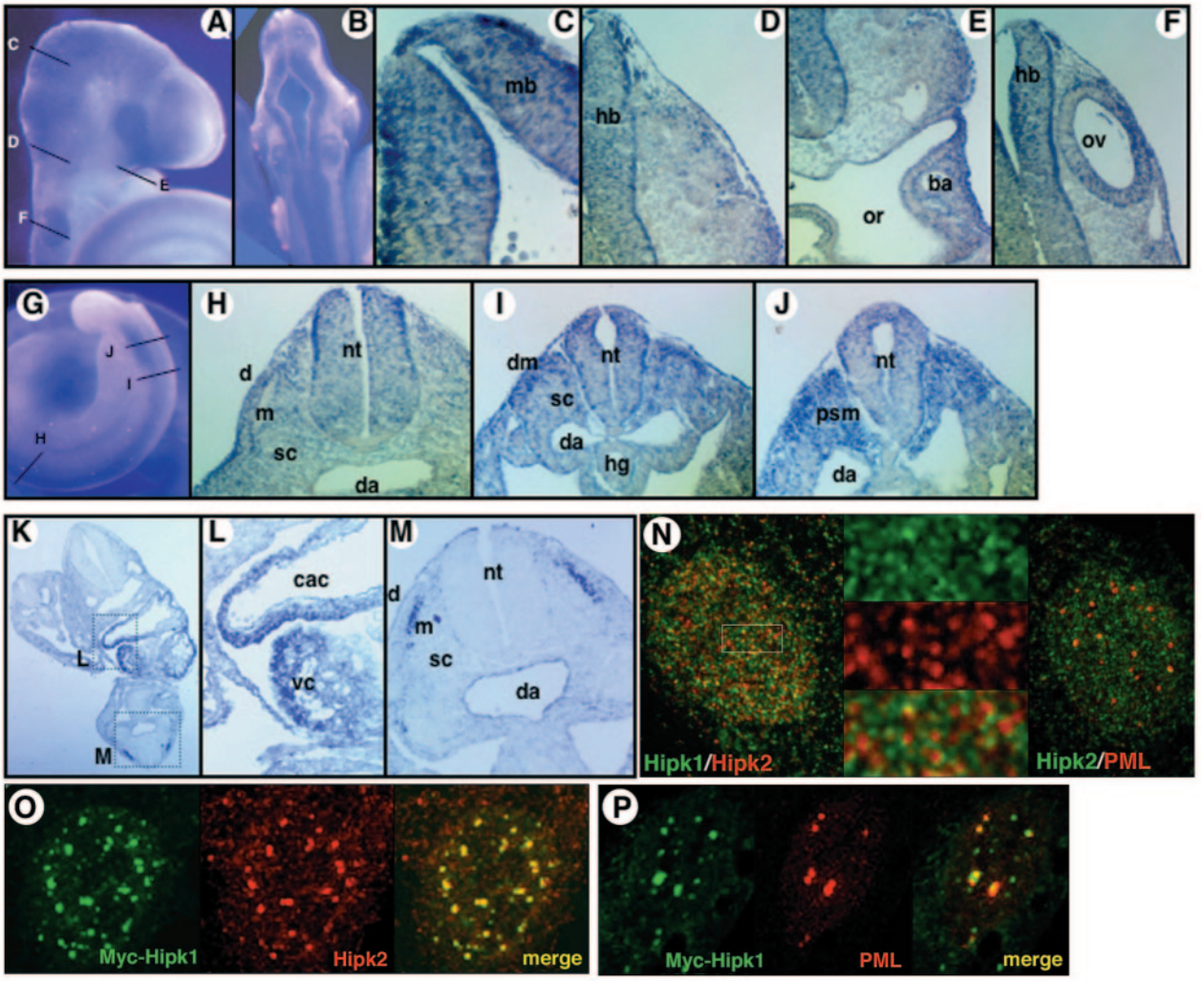

FIG. 1. Expression of *Hipk2* and *Hipk3* in 9.5 dpc embryos, and subnuclear localization of Hipk1 and Hipk2. (A) Lateral view of *Hipk2* expression in the cranial region. Note the intense expression in the neural tissue, including optic vesicle, mid- and hindbrains, and otic vesicle, compared with the weaker expression in the mesodermal tissue. The sections that are shown in panels C, D, E and F are indicated. (B) Dorsal view of *Hipk2* expression in the cranial region. (C) *Hipk2* expression at the level of midbrain (mb). Note the intense expression in the migrating neural crest cells. (D) *Hipk2* expression at the level of hindbrain (hb). (E) *Hipk2* expression around the oropharynx (or) and first branchial arch (ba). (F) *Hipk2* expression at the level of the otic vesicle (ov). (G) Lateral view of *Hipk2* expression in the caudal region. Note the intense expression in the presomitic mesoderm and first somite. The sections shown in panels H, I, and J are indicated. (H) *Hipk2* expression at the level of the prospective interlimb region. Abbreviations: d, dermatome; da, dorsal aorta; m, myotome; nt, neural tube; sc, sclerotome. (I) *Hipk2* expression at the level of de-epithelizing somite. Abbreviations: dm, dermomyotome; hg, hindgut. (J) *Hipk2* expression at the level of presomitic mesoderm (psm). (K) Lower-magnification view of *Hipk3* expression. The regions shown in panels L and M are indicated by boxes. (L) Higher-magnification view of *Hipk3* expression. Abbreviations: cac, common atrial chamber of the heart; vc, ventricular chamber of the heart. (M) Higher-magnification view of *Hipk3* expression. (N) Coexpression of Hipk1 and Hipk2 in primary MEFs. (Left) Coexpression of endogenous Hipk1 (green) and Hipk2 (red) in a MEF. (Middle) Higher-magnification views of the framed region in the left panel: endogenous Hipk1 (top), endogenous Hipk2 (middle), and merged image (bottom). (Right) A minor fraction of endogenous Hipk2 (green) is localized in PML bodies (red). (O) Subcellular localization of transfected Myc-tagged Hipk1 (left, green) and Hipk2 (middle, red) in U2OS cells. A merged image is shown in the right panel (yellow). (P) Subcellular localization of transfected Myc-tagged Hipk1 (left, green) and endogenous PML (middle, red) in U2OS cells. A merged image is shown in the right panel (yellow).

gestation against their expected values predicted by Mendelian fashion (Table 1). We next examined at which stage of gestation *Hipk1*$^{-/-}$ *Hipk2*$^{-/-}$ embryos were affected. *Hipk1*$^{-/-}$ *Hipk2*$^{+/-}$ mice which were grossly normal and fertile were mated, and the embryos were visually inspected under the stereomicroscope at 8.5, 9.5, 10.5, and 12.5 dpc (Table 2). *Hipk1*$^{-/-}$ *Hipk2*$^{-/-}$ embryos were indistinguishable from the single homozygotes at 8.5 dpc. At 9.5 dpc, however, 7 out of 24 were dead and being absorbed, and 14 out of 17 live embryos were smaller and developmentally delayed compared to *Hipk1*$^{-/-}$ *Hipk2*$^{+/+}$ or *Hipk1*$^{-/-}$ *Hipk2*$^{+/-}$ embryos. Most of the double homozygous mutants were dead before 12.5 dpc.

About half of the surviving *Hipk1*$^{-/-}$ *Hipk2*$^{-/-}$ and a small subset of the *Hipk1*$^{-/-}$ *Hipk2*$^{+/-}$ embryos failed to close the anterior neuropore and exhibited exencephaly at 9.5 and 11.5 dpc (Fig. 3A, B, and C; Table 3). This defect was characterized

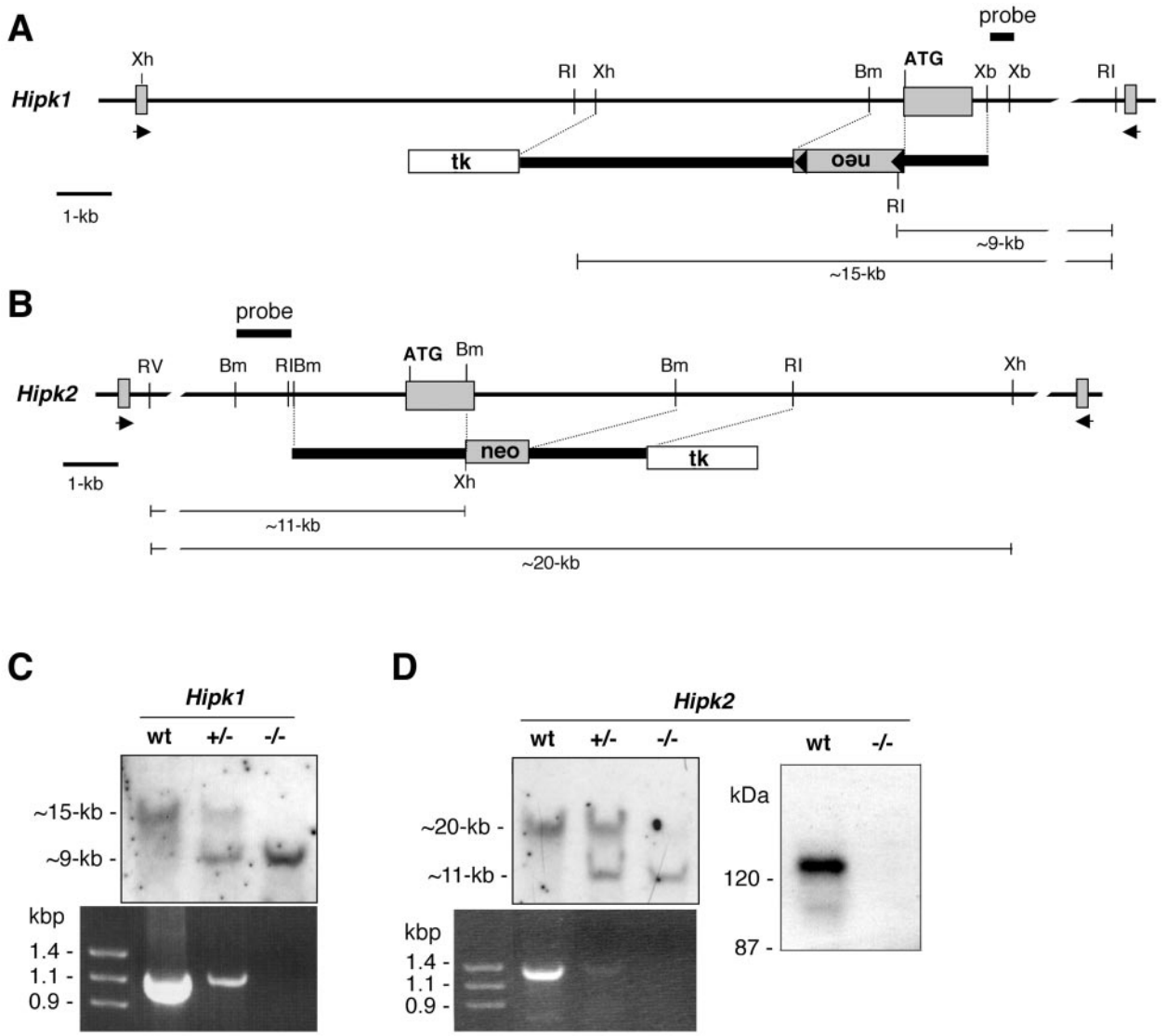

FIG. 2. Generation of *Hipk1* and *Hipk2* mutant alleles. (A and B) Genomic organization of the *Hipk1* and *Hipk2* loci around the exon containing the start codon (ATG) and their targeting constructs. Exonic regions are shown by shaded boxes. The position of each external probe (probe) is indicated. Arrowheads indicate primers used for RT-PCR. Abbreviations: neo, neomycin-resistant gene cassette; tk, herpes simplex virus thymidine kinase gene; Bm, BamHI; RI, EcoRI; RV, EcoRV; Xb, XbaI; Xh, XhoI. (C) Top: Southern blot analysis of *Hipk1* mutant allele. Genomic DNAs from respective genotypes are digested with EcoRI and probed. Bottom: RT-PCR analysis of *Hipk1* mRNA with total RNAs from 12.5 dpc embryos. wt, wild type. (D) Top left: Southern blot analysis of *Hipk2* mutant allele. Genomic DNAs from respective genotypes are digested with EcoRV and XhoI and probed. Bottom left: RT-PCR analysis of *Hipk2* mRNA with total RNAs from 12.5 dpc embryos. Right: IP-Western blot analysis of Hipk2 gene products in the wild-type (wt) and homozygous mutant (−/−) embryos at 11.5 dpc. Precipitates of anti-Hipk2 antibody were blotted with the Hipk2 antibody.

by an overgrowth of neural tissue, usually confined to the region of the fore- and midbrain but occasionally affecting the hindbrain (Fig. 3B and C). Apart from this particular neurological defect, we observed failure in lens vesicle formation associated with disorientation of optic cups and fusion of dorsal root ganglia (DRG) (Fig. 3D and E). Since embryonic survival was influenced by the dosage of *Hipk* mutations, we addressed whether *Hipk* dosage affects the incidence of neural tube closure defect (NTD) as well. Therefore, we crossed *Hipk* compound mutants and examined *Hipk* genotypes at 10.5 and 11.5 dpc, because the anterior neuropore closes during the 15- to 20-somite stage. In addition, we examined the gender effect,

TABLE 1. Survival of *Hipk* compound mutant mice[a]

Genotype	No. of mice	
	Born	Expected
$Hipk1^{+/+}$ $Hipk2^{+/+}$	11	9.5
$Hipk1^{+/-}$ $Hipk2^{+/+}$	29	19
$Hipk1^{+/+}$ $Hipk2^{+/-}$	21	19
$Hipk1^{-/-}$ $Hipk2^{+/+}$	13	9.5
$Hipk1^{+/+}$ $Hipk2^{-/-}$	9	9.5
$Hipk1^{+/-}$ $Hipk2^{+/-}$	42	38
$Hipk1^{-/-}$ $Hipk2^{+/-}$	19	19
$Hipk1^{+/-}$ $Hipk2^{-/-}$	8	19
$Hipk1^{-/-}$ $Hipk2^{-/-}$	0	9.5

[a] Mating type: $Hipk1^{+/-}$ $Hipk2^{+/-}$ × $Hipk1^{+/-}$ $Hipk2^{+/-}$.

TABLE 2. Survival of *Hipk1*$^{-/-}$ *Hipk2*$^{-/-}$ embryos during gestation[a]

Genotype	No. of live embryos (no. of embryos being resorbed) at indicated dpc:			
	8.5	9.5	10.5	12.5
Hipk1$^{-/-}$ *Hipk2*$^{+/+}$	7 (0)	34 (2)	22 (2)	14 (0)
Hipk1$^{-/-}$ *Hipk2*$^{+/-}$	12 (0)	43 (3)	30 (4)	23 (0)
Hipk1$^{-/-}$ *Hipk2*$^{-/-}$	5 (0)	24 (7)	12 (7)	1 (5)

[a] Mating type: *Hipk1*$^{-/-}$ *Hipk2*$^{+/-}$ × *Hipk1*$^{-/-}$ *Hipk2*$^{+/-}$.

as the incidence of NTD tends to be higher in females than in males (3, 35, 59). The incidence of NTD in the various *Hipk* mutants had not fully penetrated, even in the *Hipk1*$^{-/-}$ *Hipk2*$^{-/-}$ embryos, although the differences were significant and its penetrance was clearly affected by *Hipk* gene dosage (Table 3). For all genotypes, NTD occurred more frequently in females than in males. We also found that Hipk2 plays a more dominant role than Hipk1 in the suppression of NTD as well as in embryonic survival. Therefore, *Hipk1* and *Hipk2* mutations synergistically affect embryonic survival and neural tube closure.

Embryonic lethality in *Hipk1 Hipk2* double homozygotes involves p53. Female-skewed incidence of NTD has also been reported in *p53*-deficient mice, in which about 30% and 1% of homozygous females and males, respectively, exhibit exencephaly (59). Moreover, there is considerable evidence for functional interactions between HIPKs and p53 in human cells

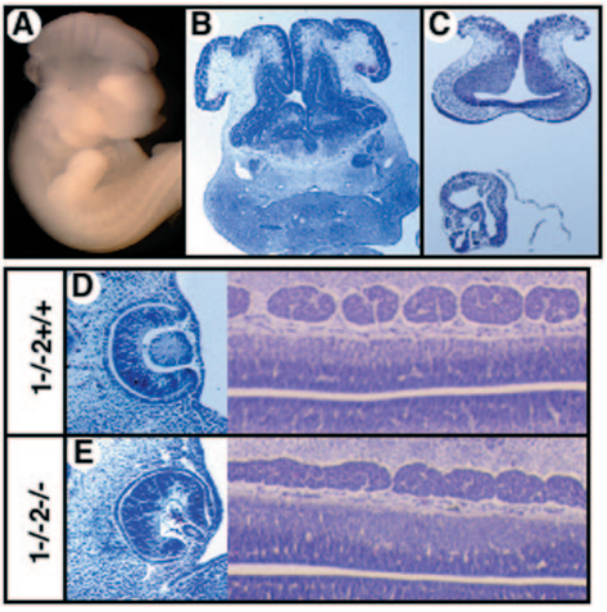

FIG. 3. Exencephaly and other histological abnormalities in *Hipk1*$^{-/-}$ *Hipk2*$^{-/-}$ embryos. (A) Lateral view of 11.5 dpc *Hipk1*$^{-/-}$ *Hipk2*$^{-/-}$ embryos exhibiting exencephaly. (B) Frontal section of 12.5 dpc *Hipk1*$^{-/-}$ *Hipk2*$^{-/-}$ embryos. (C) Frontal section of 9.5 dpc *Hipk1*$^{-/-}$ *Hipk2*$^{-/-}$ embryos. Overgrowth of neural tissue is usually confined to the region of the fore- and midbrain. (D) Normal formation of lens vesicle (left) and DRG (right) in *Hipk1*$^{-/-}$ *Hipk2*$^{+/+}$ embryos. (E) Failure of lens vesicle formation associated with disorientation of optic cups and fusion of DRGs in *Hipk1*$^{-/-}$ *Hipk2*$^{-/-}$ embryos.

TABLE 3. Incidence of NTD in male and female *Hipk* compound mutants

Genotype	Gender	NTD/total[a] (%)
Hipk1$^{-/-}$ *Hipk2*$^{+/+}$	Male	0/37 (0)
	Female	1/36 (2.8)
Hipk1$^{+/+}$ *Hipk2*$^{-/-}$	Male	0/23 (0)
	Female	1/21 (4.8)
Hipk1$^{+/-}$ *Hipk2*$^{+/-}$	Male	0/29 (0)
	Female	1/31 (3.2)
Hipk1$^{-/-}$ *Hipk2*$^{+/-}$	Male	1/62 (1.6)
	Female	5/63 (7.9)
Hipk1$^{+/-}$ *Hipk2*$^{-/-}$	Male	3/39 (7.7)
	Female	4/24 (16.7)
Hipk1$^{-/-}$ *Hipk2*$^{-/-}$	Male	11/28 (39.3)
	Female	10/18 (55.6)

[a] Number of embryos with NTD/total number of embryos with indicated genotype.

(12, 13, 14, 30, 39, 46, 57). These findings prompted us to address whether Hipks act via p53 during mouse development. Triple compound mutants were crossed to *Hipk1 Hipk2* compound mutants, and the morphology and genotype of the embryos were examined at 12.5 dpc. Four exencephalic embryos turned out to be *p53*$^{+/-}$ *Hipk1*$^{-/-}$ *Hipk2*$^{-/-}$, whereas none were *p53*$^{+/+}$ *Hipk1*$^{-/-}$ *Hipk2*$^{-/-}$; this result was surprising given the mating conditions, under which 4.5 embryos in the respective genotypes would have been expected. Although the number of samples examined was not sufficient to draw any statistical conclusions, it is possible that p53 is at least in part involved in the mediation of early embryonic lethality in *Hipk1*$^{-/-}$ *Hipk2*$^{-/-}$ embryos.

To address the molecular basis for this genetic interaction, we examined whether murine Hipk1 and Hipk2 were capable of acting together with murine p53 in the regulation of p53-dependent transcription. H1299 cells (p53$^{-/-}$) were cotransfected with expression vectors encoding human or murine p53 and murine Hipk1 or Hipk2 together with a reporter vector carrying the *p21*^{WAF1} or *Bax* promoter (Fig. 4). Both Hipk1 and Hipk2 increased p53-mediated transactivation of *p21*^{WAF1} and *Bax* promoters via murine p53 to an extent similar to that of the human counterpart. In contrast, Hipk1 or Hipk2 alone had no effect on either promoter. Therefore, Hipk1 and Hipk2 were shown to regulate p53 functions via physical interactions to mediate embryonic survival despite murine p53 lacking serine 46, which is conserved in human p53, phosphorylated by HIPK2, and involved in mediation of apoptosis upon genotoxic stimuli (14, 30, 47). Importantly, cotransfection of Hipk1 and Hipk2 did not exhibit any synergistic effects on the transactivation of p53 (Y. Li and A. Nakagawara, unpublished observations). Synergistic enhancement of respective single-mutant phenotypes in compound mutants might be due to functional redundancy or gene dosage effects rather than cooperation between Hipk1 and Hipk2.

Hipks mediate proliferation during neural and mesodermal development. In most mouse NTD models, NTDs reflect failure of neural fold elevation. Some NTD mutants, including *p53*, *Gadd45a*, and *Terc*, suggest that genes with a basic mitotic function also have a function specific to neural fold elevation (29, 34, 59). Indeed, HIPK family proteins have been shown to play significant roles in the regulation of cell growth and apop-

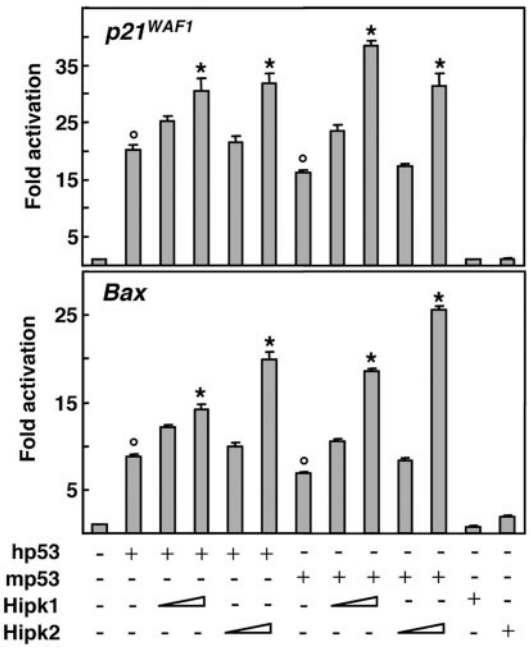

FIG. 4. Hipk1 and Hipk2 enhance p53-dependent transactivation of $p21^{WAF1}$ and *Bax* promoters via murine p53. p53-deficient H1299 cells were transiently cotransfected with the expression plasmid for human p53 (hp53) or murine p53 (mp53) along with luciferase reporter constructs containing $p21^{WAF1}$ (top) or *Bax* (bottom) promoter in the absence or presence of increasing amounts of transfected Hipk1 or Hipk2. Transfection efficiency was standardized against *Renilla* luciferase. The average relative luciferase activities in triplicate experiments are represented by bars. Means ± standard deviations of results are shown as fold induction of luciferase activity compared with number of cells transfected with vacant pcDNA3. Data shown are representative of three independent experiments with similar results. The significance of the differences were evaluated by the Student's *t* test. The bars marked with asterisks indicate significant difference ($P < 0.05$) from the bars indicated by open circles.

tosis in cultured cells and in primary sensory neurons (14, 15, 30, 39, 65). Therefore, we hypothesized that NTD in $Hipk1^{-/-}$ $Hipk2^{-/-}$ embryos may involve changes in cell growth in developing neural tube and paraxial mesoderm because the neural tube closure involves not only the neuroectoderm but also the underlying paraxial mesoderm. We first examined cellular proliferation by labeling 9.5 dpc embryos by BrdU around the level of midbrain/hindbrain boundary and prospective cervicothoracic boundary. We crossed $Hipk1^{-/-}$ $Hipk2^{+/-}$ mice and compared $Hipk1^{-/-}$ $Hipk2^{+/+}$ and $Hipk1^{-/-}$ $Hipk2^{-/-}$ embryos because *Hipk1* single mutants were morphologically normal. In the cranial region, the frequency of mitotic cells in the $Hipk1^{-/-}$ $Hipk2^{-/-}$ neural tube was significantly reduced to 45% and 29% of that of the $Hipk1^{-/-}$ embryos in the dorsal and ventral regions, respectively (Fig. 5A, B, E, F, and I). Proliferation of the cephalic mesoderm of the $Hipk1^{-/-}$ $Hipk2^{-/-}$ embryos was also reduced to 43% of the $Hipk1^{-/-}$ embryos. In the trunk region, proliferation was affected in the ventral but not the dorsal region of the neural tube and in the sclerotomal compartment of the paraxial mesoderm in the $Hipk1^{-/-}$ $Hipk2^{-/-}$ embryos (Fig. 5C, D, G, H, and J). We next investigated the frequency of apoptotic cells in the $Hipk1^{-/-}$ $Hipk2^{+/+}$ and $Hipk1^{-/-}$ $Hipk2^{-/-}$ embryos by TUNEL staining. Although we did not see a significant difference within the neural tube in the cranial region, numbers of apoptotic cells were significantly increased in the condensing trigeminal and facioacoustic neural crest cells (Fig. 5K). In the trunk region, we reproducibly observed more apoptotic outbursts in the sclerotomal compartment in $Hipk1^{-/-}$ $Hipk2^{-/-}$ than $Hipk1^{-/-}$ $Hipk2^{+/+}$ embryos but did not see significant changes in the neural tube. Therefore, Hipks are shown to promote mitosis and repress apoptotic outbursts in a tissue-specific manner during embryogenesis, which could partly be the cause of the defects in neural fold elevation. Interestingly, the fusion of DRGs is caused by an insufficient proliferation of sclerotomal cells, which may fail to provide the mesenchymal cells that separate DRGs, or by defects in craniocaudal specification of the somitic mesoderm (50, 58, 62). Craniocaudal specification and subsequent segmentation of the somites occurs normally, as revealed by the expression of *Uncx4.1* and *Hes5* in $Hipk1^{-/-}$ $Hipk2^{-/-}$ embryos (K. Isono, unpublished). Therefore, DRG fusion may also be at least in part due to impaired proliferation of sclerotomal cells.

Defective *Pax1* induction by Shh in *Hipk* double mutants. We next examined the expression of genes involved in the incidence of NTD in $Hipk1^{-/-}$ $Hipk2^{-/-}$ embryos. It is particularly interesting to investigate the expression of *Twist*, *Shh*, and Shh-dependent genes like *Pax1* and *Pax3* (5, 6, 22). Cranial NTD in *Twist* homozygotes was associated with the reduction of proliferation and expansion of the cranial mesenchyme. Shh is a predominant signaling molecule involved in neural fold elevation, which mediates the proliferation and differentiation of the neural tube and paraxial mesoderm by inducing a series of transcriptional regulators in the ventral regions of the respective tissues (22, 56). We further examined the expression of *Pax1*, which is expressed in the sclerotome in a Shh-dependent manner and is involved in the mediation of the proliferation of sclerotomal cells (22, 62). NTD in the *Pax3* mutant was shown to involve p53, and *Pax3* expression is repressed in the ventral region of the neural tube and paraxial mesoderm by Shh (20, 49).

In the wild-type and $Hipk1^{-/-}$ embryos at 9.5 dpc, *Twist* is expressed in the branchial arches and paraxial and lateral plate mesoderm (Fig. 6A, left). In $Hipk1^{-/-}$ $Hipk2^{-/-}$ embryos, the expression was significantly reduced in the paraxial and lateral plate mesoderms but not in the branchial arches (Fig. 6A, right). *Shh* expression was not significantly changed in the notochord of $Hipk1^{-/-}$ $Hipk2^{-/-}$ embryos but was reduced in the floor plate (Fig. 6B, bottom). Sclerotomal expression of the *Pax1* gene was decreased in $Hipk1^{-/-}$ $Hipk2^{-/-}$ embryos while the expression in the pharyngeal pouches was not significantly changed (Fig. 6B, top). The expression of *Pax3* in the dorsal regions of fore-, mid-, and hindbrain was not grossly changed in $Hipk1^{-/-}$ $Hipk2^{-/-}$ embryos irrespective of exencephaly (K. Isono, unpublished). However, we observed that in the neural tube in $Hipk1^{-/-}$ $Hipk2^{-/-}$ embryos, the *Pax3* expression domain was ventrally expanded (Fig. 6C). Since the expression of *Pax1* and *Pax3* in the paraxial mesoderm and/or neural tube are regulated by Shh, it is likely that Shh signaling is affected in $Hipk1^{-/-}$ $Hipk2^{-/-}$ embryos. To exclude the possibility that the expression of Shh gene products is reduced in double homozygotes, we monitored the expression of *Foxa2* in the floor plate, which is also Shh dependent (56) (Fig. 6D). *Foxa2*

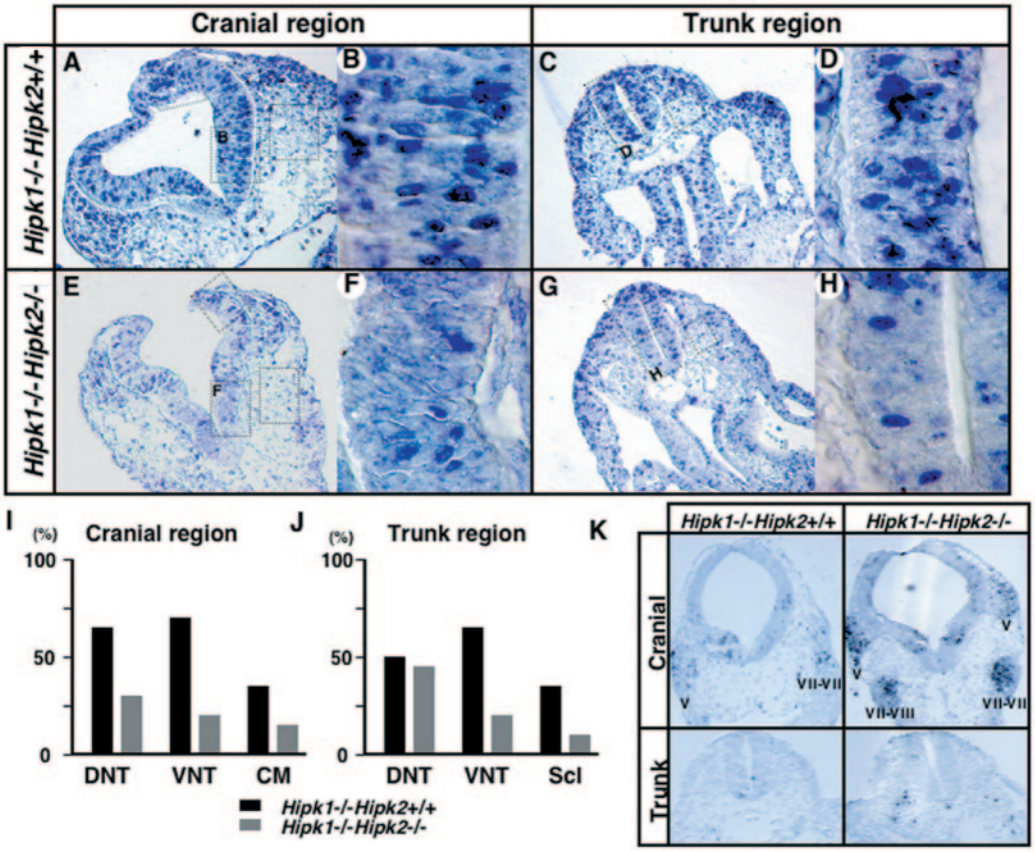

FIG. 5. Reduced mitotic cells and increased apoptotic cells in *Hipk1*$^{-/-}$ *Hipk2*$^{-/-}$ embryos. (A) Distribution of BrdU-positive cells in the cranial region of *Hipk1*$^{-/-}$ *Hipk2*$^{+/+}$ embryos at 9.5 dpc. Frequencies of BrdU-labeled cells were counted in the boxes in the dorsal region of the neural tube (DNT in panels I and J), ventral region of the neural tube (VNT in panels I and J, with a higher magnification shown in panel B) and cephalic mesoderm (CM in panels I and J). (B) Higher magnification of the area indicated by box B in panel A. (C) Distribution of BrdU-positive cells in the prospective trunk regions of *Hipk1*$^{-/-}$ *Hipk2*$^{+/+}$ embryos at 9.5 dpc. Frequencies of BrdU-labeled cells were counted in the boxes in the dorsal region of the neural tube (DNT in panels I and J), ventral region of the neural tube (VNT in panels I and J, with a higher magnification shown in panel D) and sclerotome (Scl in panels I and J). (D) Higher magnification of the area indicated by box D in panel C. (E) Distribution of BrdU-positive cells in the cranial regions of *Hipk1*$^{-/-}$ *Hipk2*$^{-/-}$ embryos at 9.5 dpc. The frequency of BrdU-labeled cells was counted in the areas demarcated by the boxes. (F) Higher magnification of the area indicated by box F in panel E. (G) Distribution of BrdU-positive cells in the prospective interlimb regions of *Hipk1*$^{-/-}$ *Hipk2*$^{-/-}$ embryos at 9.5 dpc. (H) Higher magnification of the area indicated by box H in panel G. (I) Frequency of BrdU-labeled cells in the regions indicated by boxes in the cranial region. DNT, dorsal region of the neural tube; VNT, ventral region of the neural tube; CM, cephalic mesoderm. Means are shown by black (*Hipk1*$^{-/-}$ *Hipk2*$^{+/+}$) and gray (*Hipk1*$^{-/-}$ *Hipk2*$^{-/-}$) bars. (J) Frequency of BrdU-labeled cells in the regions indicated by boxes in the prospective trunk region. Scl, sclerotome. (K) Distribution of apoptotic cells revealed by TUNEL staining in the cranial (top) and prospective trunk (bottom) regions. In the cranial region, sections through the trigeminal (V) and facioacoustic (VII-VIII) neural crest tissues are shown although the section of *Hipk1*$^{-/-}$ *Hipk2*$^{+/+}$ embryo (top left) is oblique. Note the significant apoptotic outbursts in the trigeminal and facioacoustic neural crest tissues of the *Hipk1*$^{-/-}$ *Hipk2*$^{-/-}$ embryo (top right). In the prospective trunk region, apoptotic outbursts are more pronounced in the sclerotomal compartments in the *Hipk1*$^{-/-}$ *Hipk2*$^{-/-}$ embryo (bottom right) than the *Hipk1*$^{-/-}$ *Hipk2*$^{+/+}$ embryo (bottom left).

expression was not changed in the floor plate or the midgut endoderm. Therefore, it is likely that the notochordal expression of Shh protein is unaffected in *Hipk1*$^{-/-}$ *Hipk2*$^{-/-}$ embryos. To examine whether cellular responses might be primarily impaired upon Shh signaling, we cultured explants of unsegmented paraxial mesoderm, as described previously, in the presence of Shh and investigated the *Pax1* expression in *Hipk1*$^{-/-}$ *Hipk2*$^{-/-}$ embryos (20, 21). Shh clearly induced *Pax1* expression in the micromass culture of wild-type presomitic mesoderm (Fig. 6E, left). In contrast, Shh-dependent expression of *Pax1* was totally abolished in the paraxial mesoderm derived from *Hipk1*$^{-/-}$ *Hipk2*$^{-/-}$ embryos (Fig. 6E, right), suggesting that Shh signaling to the *Pax1* induction was impaired. The expression of *Twist* was also reduced to about half that of the wild type. We did not see a significant reduction of *Pax1* expression in either single mutant (H. Koseki, unpublished). Therefore, it is likely that Hipk1 and Hipk2 are involved in the mediation of Shh-dependent proliferation of the paraxial mesoderm at least in part via transcriptional regulation of *Pax1* (6, 22).

Regulation of *Hox* gene expression by Hipks. HIPK1 and HIPK2 are capable of binding to the homeodomains of not only NK classes but also *Hox* cluster genes (37). Evidence for autoregulation of *Hoxa4* and *Drosophila Deformed* (4, 48) suggested the involvement of Hipks in the expression of *Hox* genes. This possibility was further supported by the following

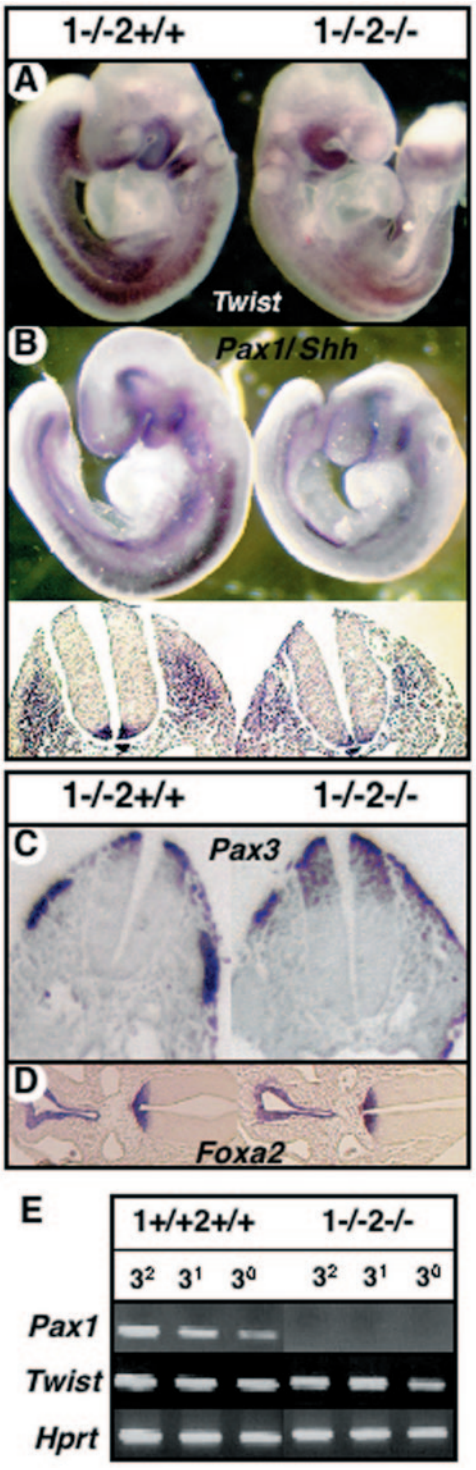

FIG. 6. Changes in Shh-dependent gene expression in the paraxial mesoderm and neural tube of *Hipk1*$^{-/-}$ *Hipk2*$^{-/-}$ embryos. (A) Expression of *Twist* in *Hipk1*$^{-/-}$ *Hipk2*$^{+/+}$ (left) and *Hipk1*$^{-/-}$ *Hipk2*$^{-/-}$ (right) embryos at 9.5 dpc. (B) Expression of *Pax1* and *Shh* in *Hipk1*$^{-/-}$ *Hipk2*$^{+/+}$ (left) and *Hipk1*$^{-/-}$ *Hipk2*$^{-/-}$ (right) embryos at 9.5 dpc. Whole-mount in situ hybridization (top) revealed significant reduction of Pax1 expression in *Hipk1*$^{-/-}$ *Hipk2*$^{-/-}$ (top right). Sections of the prospective cervical regions are shown (bottom). (C) Expression of *Pax3* in the prospective cervical regions of *Hipk1*$^{-/-}$ *Hipk2*$^{+/+}$ (left) and *Hipk1*$^{-/-}$ *Hipk2*$^{-/-}$ (right) embryos at 9.5 dpc. (D) Expression of *Foxa2* at the midgut level of *Hipk1*$^{-/-}$ *Hipk2*$^{+/+}$ (left) and *Hipk1*$^{-/-}$ *Hipk2*$^{-/-}$ (right) embryos at 9.5 dpc. (E) Impaired *Pax1* induction by Shh in explant culture of presomitic mesoderm from 9.5 dpc *Hipk1*$^{-/-}$ *Hipk2*$^{-/-}$ embryos. Total RNA extracted from the explant culture of presomitic mesoderm from wild-type (left) and *Hipk1*$^{-/-}$ *Hipk2*$^{-/-}$ (right) embryos were reverse transcribed and subjected to PCR for *Pax1* and *Twist*, with *hprt* used as a control.

observations. CRE-binding protein, which interacts with Hipk2, was shown to be involved in the regulation of *Hox* gene expression via binding to the *Hox* gene promoters (54). Furthermore, Hipk2 was demonstrated to be activated by Wnt signaling, which was also shown to impact *Hox* gene expression, in cultured cells (36, 41). Therefore, we examined the expression of *Hox* genes and the anterior-posterior specification of the axial skeleton in *Hipk* mutants. Sixty-nine and 20% of *Hipk1*$^{-/-}$ *Hipk2*$^{+/-}$ and *Hipk1*$^{+/-}$ *Hipk2*$^{-/-}$ mice, respectively, possessed ectopic ribs associated with the seventh cervical vertebra (C7) and missed the prominent spinous process from the second thoracic vertebra (T2), which may represent posterior transformations around the cervicothoracic boundary (Fig. 7A and B). The ectopic ribs were present in the single homozygotes with lower penetrance, whereas there were no changes in single heterozygotes (Fig. 7C). Therefore, Hipk1 and Hipk2 synergistically regulate the segmental identity. Next, we examined the *Hox* gene expression in the paraxial mesoderm and neural tube. In the paraxial mesoderm, no obvious changes were observed in *Hoxb6* or *Hoxb8* expression, which demarcates the prospective cervicothoracic boundary, in 11.5 dpc *Hipk1*$^{-/-}$ *Hipk2*$^{-/-}$ embryos (H. Koseki, unpublished). We went on to analyze the expression of *Hox* genes at 9.5 dpc, particularly in the neural tube. *Hoxb1* is predominantly expressed in rhombomere 4 (r4) and in the prospective spinal cord in the wild type (Fig. 7D). We found groups of *Hoxb1*-expressing cells in the r6 region in *Hipk1*$^{+/-}$ *Hipk2*$^{+/-}$ and *Hipk1*$^{-/-}$ *Hipk2*$^{-/-}$ embryos (Fig. 7E and F). The *Hoxb6* expression in the dorsal neural tube was seen up to the level of the fourth myotome in the wild type (Fig. 7G). This expression was extended to the level of the third myotome in *Hipk1*$^{-/-}$ *Hipk2*$^{-/-}$ embryos (Fig. 7H). In contrast, the expression of *Hoxa1*, *Hoxa2*, or *Hoxb3* was not changed in *Hipk1*$^{-/-}$ *Hipk2*$^{-/-}$ embryos (K. Isono, unpublished). Therefore, this suggests that Hipk1 and Hipk2 regulate the expression of a subset of *Hox* cluster genes during embryogenesis. It is possible that derepression of *Hox* expression in *Hipk* compound mutants may involve an interaction between Hox proteins and Hipk gene products. Otherwise, considering that Hipks act as repressors with histone deacetylase complexes (7, 37), Hipk1 and Hipk2 might regulate *Hox* expression at the transcription level. Whatever the intrinsic mechanisms that operate to maintain *Hox* gene expressions, *Hox* gene expressions are known to be regulated by various morphogenetic signals that include Wnts, retinoic acids, Notch signals, fibroblast growth factors, and maybe others (10, 41, 67). Derepression of *Hox* cluster genes in *Hipk* mutants might be another indication for the role of Hipks to integrate various signals and mediate appropriate cell growth to accomplish normal organ development.

The role of Hipks for activation of cell cycle checkpoints in embryonic cells. Previous studies using human tumor cell lines

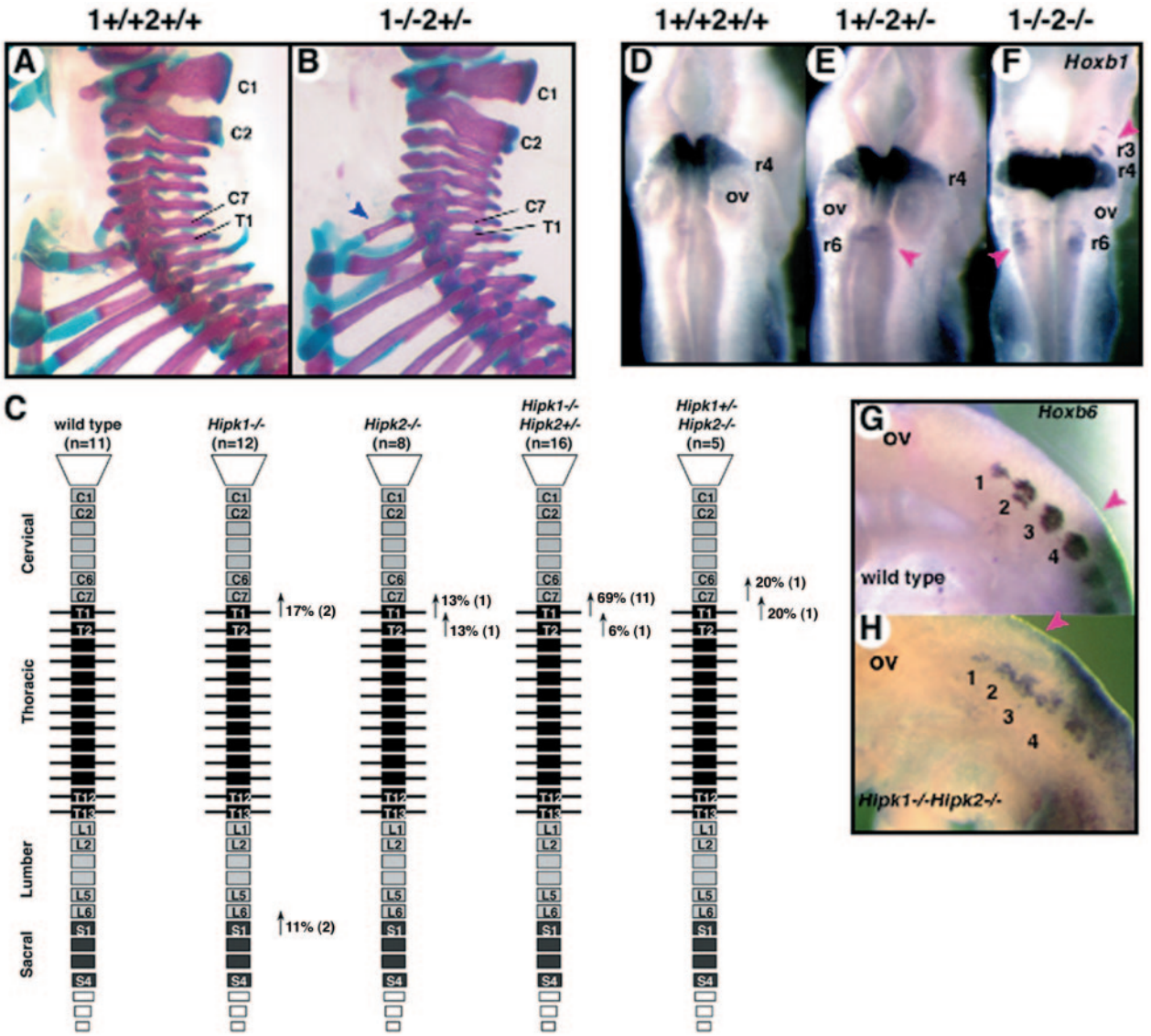

FIG. 7. Homoeotic transformations of the axial skeleton and ectopic expressions of *Hoxb1* and *Hoxb6* in the neural tubes of *Hipk1*$^{-/-}$ *Hipk2*$^{-/-}$ embryos. (A) Lateral view of the cervicothoracic region of a newborn *Hipk1*$^{+/+}$ *Hipk2*$^{+/+}$ mouse. Abbreviations: C1, first cervical vertebra; C2, second cervical vertebra; C7, seventh cervical vertebra; T1, first thoracic vertebra. (B) Lateral view of the cervicothoracic region of a newborn *Hipk1*$^{-/-}$ *Hipk2*$^{-/-}$ mouse. An ectopic rib associated with C7 is indicated by the blue arrowhead. (C) Summary of homoeotic transformations of axial skeleton. The numbers of affected individuals are shown in parentheses. T1→C7 transformation is characterized by the ectopic rib associated with C7. T2→T1 transformation is characterized by the shift of the prominent spinous process from T2 to T1. C7→C6 transformation is characterized by the lack of anterior processes from C6 and the concomitant appearance of the anterior process on C5. S1→L6 transformation is characterized by the sacroiliac joint in L6. (D) Expression of *Hoxb1* in *Hipk1*$^{+/+}$ *Hipk2*$^{+/+}$ embryos at 9.5 dpc. Note that the expression is localized to rhombomere 4 (r4) and the prospective spinal cord. ov, otic vesicle. (E) Expression of *Hoxb1* in *Hipk1*$^{+/-}$ *Hipk2*$^{+/-}$ embryos at 9.5 dpc. Note the subtle derepression in rhombomere 6 (r6), which is indicated by an arrowhead. (F) Expression of *Hoxb1* in *Hipk1*$^{-/-}$ *Hipk2*$^{-/-}$ embryos at 9.5 dpc. Note the derepression in rhombomere 3 (r3) and r6, which are indicated by arrowheads. (G) Expression of *Hoxb6* in *Hipk1*$^{+/+}$ *Hipk2*$^{+/+}$ embryos at 9.5 dpc. Positions of somites are visualized by *myogenin* expression, and each segment is numerically indicated. The anterior boundary of *Hoxb6* expression in the neural tube is indicated by an arrowhead. (H) Expression of *Hoxb6* in *Hipk1*$^{-/-}$ *Hipk2*$^{-/-}$ embryos at 9.5 dpc. Note that the anterior boundary is shifted to the level of the third somite.

have shown that HIPK1 and HIPK2 were involved in mediating DNA damage-induced apoptosis or cell cycle arrest by regulating the p53 and/or CtBP (14, 30, 38, 68, 69). If this is also the case in primary embryonic cells, it is hypothesized that Hipk1 and Hipk2 are involved in eliminating proliferating progenitors with genetic instability, which may in turn guarantee normal organ development and homeostasis. We therefore examined cellular growth upon genotoxic insult by using proliferating primary MEFs generated from 12.5 dpc fetuses, apart from the double homozygotes, which die at an earlier stage. We tested the UV response of MEFs with mutations in *Hipk* and p53$^{-/-}$, as a reference. The numbers of dead and living cells were counted 6, 11, and 24 h after UV (50 J/m^2) exposure. *Hipk1* and *Hipk2* single-mutant MEFs were slightly

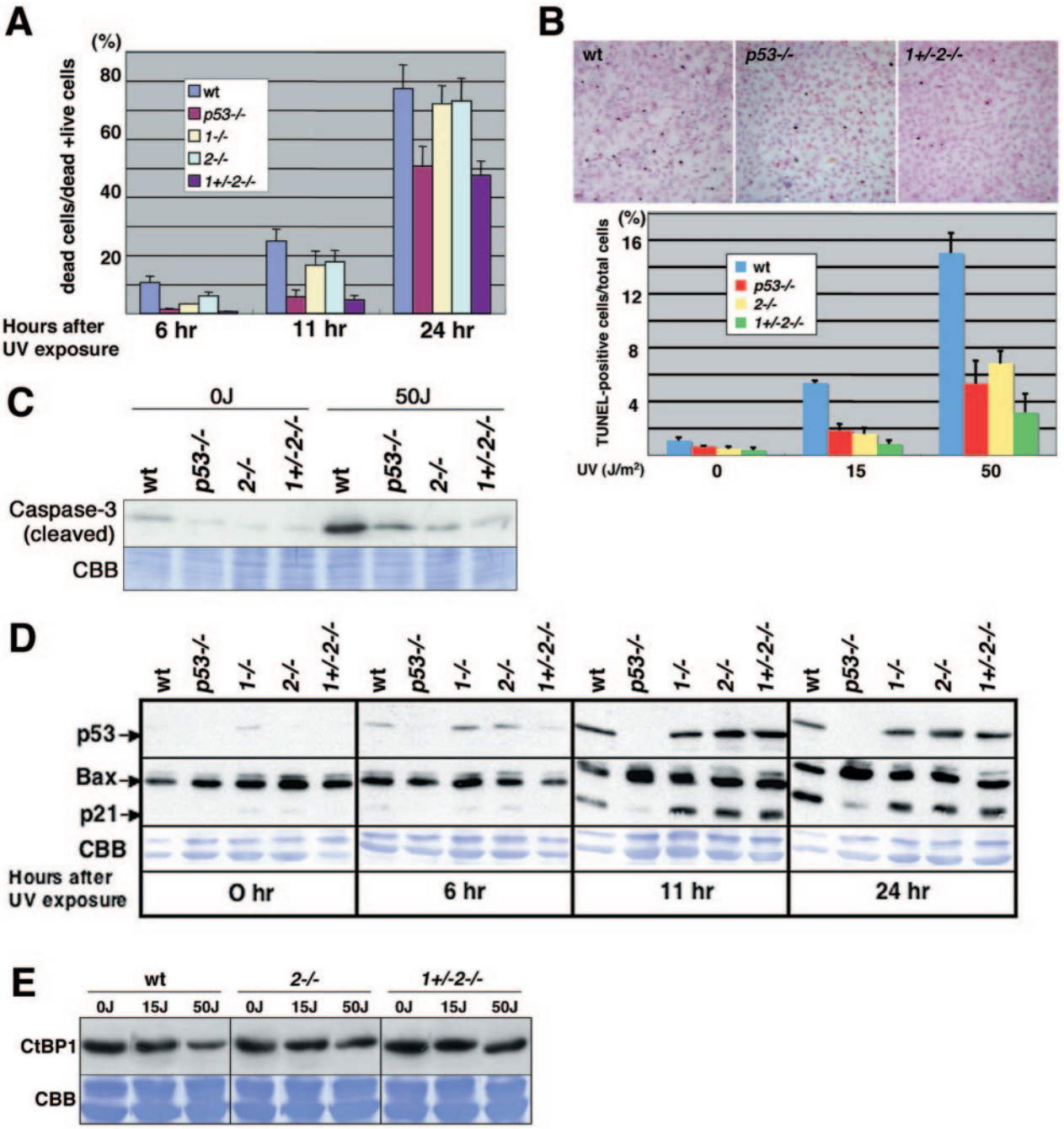

FIG. 8. Hipks mediate UV-induced apoptosis in primary MEFs. (A) Frequency of dead cells 6, 11, and 24 h after UV irradiation as revealed by trypan blue exclusion. Means ± standard deviations are shown by bars for the respective genotypes. (B) Frequency of apoptotic cells 12 h after UV irradiation (15 or 50 J/m^2) as revealed by TUNEL assay. (Top) Microscopic views of TUNEL-positive cells induced by UV (15 J/m^2) in wild-type (wt; left), *p53*$^{-/-}$ (middle), and *Hipk1*$^{+/-}$ *Hipk2*$^{-/-}$ (right) MEFs. (Bottom) Frequency of apoptotic cells 12 h after UV irradiation (15 or 50 J/m^2) are summarized. Means ± standard deviations are shown by bars for the respective genotypes. (C) Western blot analyses for the cleaved form of caspase-3 in MEFs with respective genotypes. Nonirradiated MEFs were used as the 0 J control. (D) Expression of p53, Bax, and p21^{WAF1} in *Hipk* mutant MEFs 6, 11, and 24 h after UV irradiation. Nonirradiated MEFs were used as the 0 h control. After immunodetection, membranes were stained with Coomassie brilliant blue (CBB) to quantify the amounts of blotted proteins. (E) Expression of CtBP1 in *Hipk* mutant MEFs 12 h after UV irradiation (15 or 50 J/m^2).

resistant to UV exposure compared to the wild type (Fig. 8A). *Hipk1*$^{+/-}$ *Hipk2*$^{-/-}$ MEFs were more resistant than single mutants, and the frequency of dead cells was equivalent to that for *p53*$^{-/-}$ cells. This result was further confirmed by TUNEL assay and Western blotting for cleaved caspase-3, which represents apoptotic outbursts. Frequency of TUNEL-positive cells induced by UV irradiation was significantly reduced in *p53*$^{-/-}$, *Hipk2*$^{-/-}$, and *Hipk1*$^{+/-}$ *Hipk2*$^{-/-}$ MEFs compared to

the wild type (Fig. 8B). Concordantly, accumulation of cleaved caspase-3 upon UV irradiation was affected in *p53*$^{-/-}$, *Hipk2*$^{-/-}$, and *Hipk1*$^{+/-}$ *Hipk2*$^{-/-}$ MEFs (Fig. 8C). In conclusion, Hipk1 and Hipk2 were required to mediate apoptosis upon UV stress in murine proliferating MEFs as well as human tumor cell lines. Therefore, Hipks were suggested to activate cell cycle checkpoints in embryonic primary cells.

We next addressed whether the p53 or CtBP pathway was activated by Hipk1 and Hipk2 upon UV irradiation in MEFs. In UV-irradiated human tumor cells, HIPK2 activates human p53 at least via phosphorylation of serine 46, which in turn induces the apoptosis-inducible factor gene *p53AIP1* (14, 30, 47). Hipks were shown to activate murine p53-mediated transcription of *p21*^{WAF1} and *Bax* promoters, and p53 was suggested to mediate embryonic lethality in *Hipk1 Hipk2* double homozygotes (Fig. 4). However, murine p53 does not possess a serine residue equivalent to the serine 46 of human p53, and neither has a *p53AIP1* locus been found in the mouse genome (see Fig. S1 and S2 in the supplemental material). We thus examined the involvement of p53 by analyzing the expression of p53 and the two p53 targets, p21^{WAF1} and Bax, in *Hipk* mutants upon UV irradiation (18, 43). Interestingly, we did not see a significant difference in the expression of p53, p21^{WAF1}, or Bax between *Hipk* mutants and the wild type (Fig. 8D). We then examined the cellular senescence in *Hipk*-mutated MEFs since this is accompanied by accumulation of p53 gene products and cancelled by *p53* mutation (27). *Hipk1*$^{+/-}$ *Hipk2*$^{-/-}$ and *Hipk1*$^{-/-}$ *Hipk2*$^{+/-}$ MEFs senesced like the wild type in a strict 3T9 protocol while *p53*$^{-/-}$ MEFs kept on growing (K. Isono, unpublished) (27). Therefore, Hipk1 and/or Hipk2 may not mediate apoptosis or cellular senescence upon UV or mitotic stress, respectively, by stabilizing p53. However, we could not exclude other possibilities that Hipk1 and Hipk2 might activate p53 through phosphorylation of other common residues or other modifications.

We went on to analyze the expression of CtBP in *Hipk* mutant MEFs, since UV-inducible phosphorylation of human CtBP at serine 422 by HIPK2 destabilizes CtBP and the reduction of CtBP promotes apoptosis irrespective of p53 activation (68, 69). In the wild-type MEFs, UV irradiation induced a reduction of CtBP1 expression in a UV dose-dependent manner (Fig. 8E). In contrast, CtBP1 expression was not significantly decreased after UV exposure in *Hipk1*$^{+/-}$ *Hipk2*$^{-/-}$, *Hipk1*$^{-/-}$, or *Hipk2*$^{-/-}$ MEFs. Therefore, it is likely that Hipk1 and Hipk2 are involved in mediating UV-induced apoptosis by decreasing CtBP expression in MEFs, although it might be of note that the stabilized CtBP level alone cannot explain the difference of apoptotic resistance between each *Hipk* single mutant and *Hipk1*$^{+/-}$ *Hipk2*$^{-/-}$. Taken together, Hipk1 and Hipk2 are required for not only proliferation of embryonic cells upon morphogenetic signals but also activation of cell cycle checkpoints upon genotoxic stimulus during embryogenesis.

DISCUSSION

In this study, by using *Hipk1 Hipk2* compound mutants, we have shown that Hipk1 and Hipk2 act in synergy to mediate growth regulation upon morphogenetic and genotoxic signals. Since both *Hipk1* and *Hipk2* are expressed almost ubiquitously around 9.5 dpc and their products are coexpressed in the nuclei of MEFs and colocalized to subnuclear domains following overexpression, the molecular basis for this synergy is most likely due to the functional overlap between Hipk1 and Hipk2 and mutually compensative properties, although Hipk2 may exert a slightly dominant role. It is also noteworthy that embryonic survival and neural tube closure are affected in compound mutants in a gene dosage-dependent manner. This genetic interaction could imply that the total amount of Hipk protein is an important parameter in mediating the appropriate cellular responses required for normal development. Indeed, the expression level of HIPK2, which correlates in a linear fashion with the degree of DNA damage, differentially impacts the posttranslational modifications of human p53 and subsequent cellular responses (12, 13). It has also been shown that the phosphorylation and sumoylation statuses of HIPK2 are altered by various cellular inputs, which in turn affect the HIPK2 functions (32, 60). It is therefore likely that several distinct mechanisms operate to maintain the functional quantity of Hipks. In vertebrates, the presence of three structurally and functionally homologous Hipk proteins might be involved in guaranteeing that the appropriate amounts of functional Hipks are available throughout embryogenesis and in allowing postnatal survival.

Regulation of cell growth by Hipk1 and Hipk2 during embryogenesis is shown to involve not only induction of transcription factors required for morphogenetic proliferation but also activation of cell cycle checkpoints upon genotoxic stimulation. It is thus possible that activation of Hipks by various morphogenetic signals may sensitize proliferating progenitor cells for apoptotic outbursts, which may facilitate elimination of cells with genetic instability. Notably, loss of Hipks also activates checkpoints since embryonic lethality in *Hipk1*$^{-/-}$ *Hipk2*$^{-/-}$ embryos is at least partly alleviated by *p53* mutation. Therefore Hipks are tightly linked to cell cycle checkpoint mechanisms in embryonic cells and may either activate or repress their functions to mediate the appropriate cellular responses by sensing various extracellular stimuli.

It has been suggested that, by regulating the transcription of target genes such as *Pax1* and *Pax3*, Hipks mediate Shh signaling, which results in the proliferation in developing paraxial mesoderm and neural tube. This is in agreement with previous observations that HIPKs bind and activate CRE-binding protein, which is a functional component of Shh signaling (2, 9, 22). Intriguingly, HIPK2 has also been shown to negatively regulate BMP-induced transcription by inhibiting Smads (26). Since opposing long-range signals mediated by Shh and BMP4 are essential for dorsoventral specification of the neural tube and paraxial mesoderm (22, 42), Hipks may be involved in the integration of two antagonizing signals and thereby facilitate cell growth and differentiation in the ventral regions. Different cellular inputs appear to induce different modifications or alter the subcellular localization of Hipks and subsequently drive transcription of different target genes by means of differential interactions with its binding partners (60). This previous conclusion is supported by our findings that Hipk1 and Hipk2 promote UV-induced apoptosis in MEFs but repress apoptotic outbursts in some differentiating tissues. The most attractive scenario for this integrating role of Hipks during the dorsoventral specification is that a certain alteration of Hipks in-

duced by Shh signaling may facilitate the formation of a repressive complex with Ski and Smads, which may in turn inhibit the BMP4 signaling cascade. Previous studies have demonstrated that HIPKs were capable of responding to a vast range of extracellular signals (60). It is possible that Hipks may play this integrating role during the induction and/or maintenance of *Hox* gene expressions, which are mediated by a combination of various signaling molecules including at least Wnts, retinoic acid, Notch, and fibroblast growth factors (10, 41, 67). Taken together, Hipks integrate these signals in order to mediate between the appropriate growth responses during development and cellular homeostasis. It is notable that functional coupling has recently been found between the differentiation checkpoint mechanism and genotoxic signaling cascade during myogenesis and that this contributes to differentiation of muscle precursors (53). Hipks could be involved in the qualification of stressed cells by various extracellular inputs, which would secure the cells' further development and survival.

NTDs, particularly exencephaly and spina bifida, are common human birth defects, and their genetics are very complex. Accordingly, in mice, mutations at many loci have been shown to cause NTDs (35). The present study clearly indicated the protective roles of Hipks against NTD, particularly exencephaly. In nearly all known NTD mutants examined, NTD arises from a failure to complete the process of elevation of the neural folds to become vertical. Neural fold elevation has been shown to be dependent on the proliferation of the neural fold and/or the underlying mesoderm because reduced mitosis in these tissues is associated with NTDs in *Twist*, *Pax1*/*PDGFR*α, *Pax1*/*foxc2*, *Shh*, and *Opb* mutants (5, 6, 17, 23, 28). It is therefore likely that Hipks mediate neural fold elevation by regulating mitosis in the neural folds and/or underlying mesoderm, which may involve the Shh signaling cascade (66). It is also noteworthy that mutations in genes encoding interacting partners for Hipks, including *p53*, *Cbp*, *Axin*, and *Ski*, have been shown to cause exencephaly (35). Importantly, these have also been shown to be involved in the signaling cascades of Shh, Wnt, or BMPs (2, 8, 9, 26, 57, 61). Therefore, in conclusion, it is hypothesized that coordination of the proliferation in the subdomains of neural tube and paraxial mesoderm is required for correct neural fold elevation and that Hipks could be involved in the coordination of the mitotic responses to various morphogenetic signals (66).

ACKNOWLEDGMENTS

This project was supported by Special Coordination Funds for the Promotion of Science and Technology from the Ministry of Education, Culture, Sports, Science and Technology of the Japanese Government (H.K.).

We thank Ryoko Moriizumi, Sanae Takeda, Misao Uchida, Tamie Endo, and the late Shozo Sugimori for their help.

REFERENCES

1. **Akasaka, T., M. Kanno, R. Balling, M. A. Mieza, M. Taniguchi, and H. Koseki.** 1996. A role for Mel18, a Polycomb group-related vertebrate gene, during the anteroposterior specification of the axial skeleton. Development **122:**1513–1522.
2. **Akimaru, H., Y. Chen, P. Dai, D. X. Hou, M. Nonaka, S. M. Smolik, S. Armstrong, R. H. Goodman, and S. Ishii.** 1997. Drosophila CBP is a co-activator of cubitus interruptus in hedgehog signalling. Nature **386:**735–738.
3. **Armstrong, J. F., M. H. Kaufman, D. J. Harrison, and A. R. Clarke.** 1995. High-frequency developmental abnormalities in p53-deficient mice. Curr. Biol. **5:**931–936.
4. **Bergson, C., and W. McGinnis.** 1990. An autoregulatory enhancer element of the Drosophila homeotic gene Deformed. EMBO J. **9:**4287–4297.
5. **Chen, Z. F., and R. R. Behringer.** 1995. *Twist* is required in head mesenchyme for cranial neural tube morphogenesis. Gene Dev. **9:**689–699.
6. **Chiang, C., Y. Litingtung, E. Lee, K. E. Young, J. L. Corden, H. Westphal, and P. A. Beachy.** 1996. Cyclopia and defective axial patterning in mice lacking Sonic hedgehog gene function. Nature **383:**407–413.
7. **Choi, C. Y., Y. H. Kim, H. J. Kwon, and Y. Kim.** 1999. The homeodomain protein NK-3 recruits Groucho and a histone deacetylase complex to repress transcription. J. Biol. Chem. **274:**33194–33197.
8. **Cordenonsi, M., S. Dupont, S. Maretto, A. Insinga, C. Imbriano, and S. Piccolo.** 2003. Links between tumor suppressors: p53 is required for TGF-beta gene responses by cooperating with Smads. Cell **113:**301–314.
9. **Dai, P., H. Akimaru, Y. Tanaka, T. Maekawa, M. Nakafuku, and S. Ishii.** 1999. Sonic Hedgehog-induced activation of the Gli1 promoter is mediated by GLI3. J. Biol. Chem. **274:**8143–8152.
10. **Diez del Corral, R., and K. G. Storey.** 2004. Opposing FGF and retinoid pathways: a signalling switch that controls differentiation and patterning onset in the extending vertebrate body axis. Bioessays **26:**857–869.
11. **Di Stefano, V., G. Blandino, A. Sacchi, S. Soddu, and G. D'Orazi.** 2004. HIPK2 neutralizes MDM2 inhibition rescuing p53 transcriptional activity and apoptotic function. Oncogene **23:**5185–5192.
12. **Di Stefano, V., C. Rinaldo, A. Sacchi, S. Soddu, and G. D'Orazi.** 2004. Homeodomain-interacting protein kinase-2 activity and p53 phosphorylation are critical events for cisplatin-mediated apoptosis. Exp. Cell Res. **293:**311–320.
13. **Di Stefano, V., S. Soddu, A. Sacchi, and G. D'Orazi.** 2005. HIPK2 contributes to PCAF-mediated p53 acetylation and selective transactivation of p21(Waf1) after nonapoptotic DNA damage. Oncogene **24:**5431–5442.
14. **D'Orazi, G., B. Cecchinelli, T. Bruno, I. Manni, Y. Higashimoto, S. Saito, M. Gostissa, S. Coen, A. Marchetti, G. Del Sal, G. Piaggio, M. Fanciulli, E. Appella, and S. Soddu.** 2002. Homeodomain-interacting protein kinase-2 phosphorylates p53 at Ser 46 and mediates apoptosis. Nat. Cell Biol. **4:**11–19.
15. **Doxakis, E., E. J. Huang, and A. M. Davies.** 2004. Homeodomain-interacting protein kinase-2 regulates apoptosis in developing sensory and sympathetic neurons. Curr. Biol. **14:**1761–1765.
16. **Ecsedy, J. A., J. S. Michaelson, and P. Leder.** 2003. Homeodomain-interacting protein kinase 1 modulates Daxx localization, phosphorylation, and transcriptional activity. Mol. Cell. Biol. **23:**950–960.
17. **Eggenschwiler, J. T., E. Espinoza, and K. V. Anderson.** 2001. Rab23 is an essential negative regulator of the mouse Sonic hedgehog signalling pathway. Nature **412:**194–198.
18. **el-Deiry, W. S., T. Tokino, V. E. Velculescu, D. B. Levy, R. Parsons, J. M. Trent, D. Lin, W. E. Mercer, K. W. Kinzler, and B. Vogelstein.** 1993. WAF1, a potential mediator of p53 tumor suppression. Cell **75:**817–825.
19. **Engelhardt, O. G., C. Boutell, A. Orr, E. Ullrich, O. Haller, and R. D. Everett.** 2003. The homeodomain-interacting kinase PKM (HIPK-2) modifies ND10 through both its kinase domain and a SUMO-1 interaction motif and alters the posttranslational modification of PML. Exp. Cell Res. **283:**36–50.
20. **Epstein, D. J., M. Vekemans, and P. Gros.** 1991. Splotch (Sp2H), a mutation affecting development of the mouse neural tube, shows a deletion within the paired homeodomain of Pax-3. Cell **67:**767–774.
21. **Fan, C. M., and M. Tessier-Lavigne.** 1994. Patterning of mammalian somites by surface ectoderm and notochord: evidence for sclerotome induction by a hedgehog homolog. Cell **79:**1175–1186.
22. **Fan, C. M., J. A. Porter, C. Chiang, D. T. Chang, P. A. Beachy, and M. Tessier-Lavigne.** 1995. Long-range sclerotome induction by sonic hedgehog: direct role of the amino-terminal cleavage product and modulation by the cyclic AMP signaling pathway. Cell **81:**457–465.
23. **Furumoto, T. A., N. Miura, T. Akasaka, Y. Mizutani-Koseki, H. Sudo, K. Fukuda, M. Maekawa, S. Yuasa, Y. Fu, H. Moriya, M. Taniguchi, K. Imai, E. Dahl, R. Balling, M. Pavlova, A. Gossler, and H. Koseki.** 1999. Notochord-dependent expression of MFH1 and PAX1 cooperates to maintain the proliferation of sclerotome cells during the vertebral column development. Dev. Biol. **210:**15–29.
24. **Gondo, Y., K. Nakamura, K. Nakao, T. Sasaoka, K. Ito, M. Kimura, and M. Katsuki.** 1994. Gene replacement of the p53 gene with the lacZ gene in mouse embryonic stem cells and mice by using two steps of homologous recombination. Biochem. Biophys. Res. Commun. **202:**830–837.
25. **Gresko, E., A. Moller, A. Roscic, and M. L. Schmitz.** 2005. Covalent modification of human homeodomain interacting protein kinase 2 by SUMO-1 at lysine 25 affects its stability. Biochem. Biophys. Res. Commun. **329:**1293–1299.
26. **Harada, J., K. Kokura, C. Kanei-Ishii, T. Nomura, M. M. Khan, Y. Kim, and S. Ishii.** 2003. Requirement of the co-repressor homeodomain-interacting protein kinase 2 for ski-mediated inhibition of bone morphogenetic protein-induced transcriptional activation. J. Biol. Chem. **278:**38998–39005.
27. **Harvey, M., A. T. Sands, R. S. Weiss, M. E. Hegi, R. W. Wiseman, P. Pantazis, B. C. Giovanella, M. A. Tainsky, A. Bradley, and L. A. Donehower.** 1993. In vitro growth characteristics of embryo fibroblasts isolated from p53-deficient mice. Oncogene **8:**2457–2467.

28. **Helwig, U., K. Imai, W. Schmahl, B. E. Thomas, D. S. Varnum, J. H. Nadeau, and R. Balling.** 1995. Interaction between undulated and Patch leads to an extreme form of spina bifida in double-mutant mice. Nat. Genet. **11:**60–63.
29. **Herrera, E., E. Samper, and M. A. Blasco.** 1999. Telomere shortening in mTR−/− embryos is associated with failure to close the neural tube. EMBO J. **18:**1172–1181.
30. **Hofmann, T. G., A. Moller, H. Sirma, H. Zentgraf, Y. Taya, W. Droge, H. Will, and M. L. Schmitz.** 2002. Regulation of p53 activity by its interaction with homeodomain-interacting protein kinase-2. Nat. Cell Biol. **4:**1–10.
31. **Hofmann, T. G., N. Stollberg, M. L. Schmitz, and H. Will.** 2003. HIPK2 regulates transforming growth factor-β-induced c-Jun NH_2-terminal kinase activation and apoptosis in human hepatoma cells. Cancer Res. **63:**8271–8277.
32. **Hofmann, T. G., E. Jaffray, N. Stollberg, R. T. Hay, and H. Will.** 2005. Regulation of homeodomain-interacting protein kinase 2 (HIPK2) effector function through dynamic SUMO-1 modification. J. Biol. Chem. **280:**29224–29232.
33. **Hogan, B., R. Beddington, F. Costantini, and E. Lacy.** 1994. Isolation, culture, and manipulation of embryonic stem cells, p. 253–290. *In* B. Hogan, F. Costantini, and E. Lacy (ed.), Manipulating the mouse embryo: a laboratory manual, 2nd ed. Cold Spring Harbor Laboratory Press, Cold Spring Harbor, N.Y.
34. **Hollander, M. C., M. S. Sheikh, D. V. Bulavin, K. Lundgren, L. Augeri-Henmueller, R. Shehee, T. A. Molinaro, K. E. Kim, E. Tolosa, J. D. Ashwell, M. P. Rosenberg, Q. Zhan, P. M. Fernandez-Salguero, W. F. Morgan, C. X. Deng, and A. J. Fornace, Jr.** 1999. Genomic instability in Gadd45a-deficient mice. Nat. Genet. **23:**176–184.
35. **Juriloff, D. M., and M. J. Harris.** 2000. Mouse models for neural tube closure defects. Hum. Mol. Genet. **9:**993–1000.
36. **Kanei-Ishii, C., J. Ninomiya-Tsuji, J. Tanikawa, T. Nomura, T. Ishitani, S. Kishida, K. Kokura, T. Kurahashi, E. Ichikawa-Iwata, Y. Kim, K. Matsumoto, and S. Ishii.** 2004. Wnt-1 signal induces phosphorylation and degradation of c-Myb protein via TAK1, HIPK2, and NLK. Genes Dev. **18:**816–829.
37. **Kim, Y. H., C. Y. Choi, S. J. Lee, M. A. Conti, and Y. Kim.** 1998. Homeodomain-interacting protein kinases, a novel family of co-repressors for homeodomain transcription factors. J. Biol. Chem. **273:**25875–25879.
38. **Kim, Y. H., C. Y. Choi, and Y. Kim.** 1999. Covalent modification of the homeodomain-interacting protein kinase 2 (HIPK2) by the ubiquitin-like protein SUMO-1. Proc. Natl. Acad. Sci. USA **96:**12350–12355.
39. **Kondo, S., Y. Lu, M. Debbas, A. W. Lin, I. Sarosi, A. Itie, A. Wakeham, J. Tuan, C. Saris, G. Elliott, W. Ma, S. Benchimol, S. W. Lowe, T. W. Mak, and S. K. Thukral.** 2003. Characterization of cells and gene-targeted mice deficient for the p53-binding kinase homeodomain-interacting protein kinase 1 (HIPK1). Proc. Natl. Acad. Sci. USA **100:**5431–5436.
40. **Li, X., R. Zhang, D. Luo, S. J. Park, Q. Wang, Y. Kim, and W. Min.** 2005. Tumor necrosis factor alpha-induced desumoylation and cytoplasmic translocation of homeodomain-interacting protein kinase 1 are critical for apoptosis signal-regulating kinase 1-JNK/p38 activation. J. Biol. Chem. **280:**15061–15070.
41. **Lohnes, D.** 2003. The Cdx1 homeodomain protein: an integrator of posterior signaling in the mouse. Bioessays **25:**971–980.
42. **McMahon, J. A., S. Takada, L. B. Zimmerman, C. M. Fan, R. M. Harland, and A. P. McMahon.** 1998. Noggin-mediated antagonism of BMP signaling is required for growth and patterning of the neural tube and somite. Genes Dev. **12:**1438–1452.
43. **Miyashita, T., and J. C. Reed.** 1995. Tumor suppressor p53 is a direct transcriptional activator of the human bax gene. Cell **80:**293–299.
44. **Moilanen, A. M., U. Karvonen, H. Poukka, O. A. Janne, and J. J. Palvimo.** 1998. Activation of androgen receptor function by a novel nuclear protein kinase. Mol. Biol. Cell **9:**2527–2543.
45. **Moller, A., H. Sirma, T. G. Hofmann, S. Rueffer, E. Klimczak, W. Droge, H. Will, and M. L. Schmitz.** 2003. PML is required for homeodomain-interacting protein kinase 2 (HIPK2)-mediated p53 phosphorylation and cell cycle arrest but is dispensable for the formation of HIPK domains. Cancer Res. **63:**4310–4314.
46. **Moller, A., H. Sirma, T. G. Hofmann, H. Staege, E. Gresko, K. S. Ludi, E. Klimczak, W. Droge, H. Will, and M. L. Schmitz.** 2003. Sp100 is important for the stimulatory effect of homeodomain-interacting protein kinase-2 on p53-dependent gene expression. Oncogene **22:**8731–8737.
47. **Oda, K., H. Arakawa, T. Tanaka, K. Matsuda, C. Tanikawa, T. Mori, H. Nishimori, K. Tamai, T. Tokino, Y. Nakamura, and Y. Taya.** 2000. p53AIP1, a potential mediator of p53-dependent apoptosis, and its regulation by Ser-46-phosphorylated p53. Cell **102:**849–862.
48. **Packer, A. I., D. A. Crotty, V. A. Elwell, and D. J. Wolgemuth.** 1998. Expression of the murine Hoxa4 gene requires both autoregulation and a conserved retinoic acid response element. Development **125:**1991–1998.
49. **Pani, L., M. Horal, and M. R. Loeken.** 2002. Rescue of neural tube defects in Pax-3-deficient embryos by p53 loss of function: implications for Pax-3-dependent development and tumorigenesis. Genes Dev. **16:**676–680.
50. **Peters, H., B. Wilm, N. Sakai, K. Imai, R. Maas, and R. Balling.** 1999. Pax1 and Pax9 synergistically regulate vertebral column development. Development **126:**5399–5408.
51. **Pierantoni, G. M., M. Fedele, F. Pentimalli, G. Benvenuto, R. Pero, G. Viglietto, M. Santoro, L. Chiariotti, and A. Fusco.** 2001. High mobility group I (Y) proteins bind HIPK2, a serine-threonine kinase protein which inhibits cell growth. Oncogene **20:**6132–6141.
52. **Pierantoni, G. M., A. Bulfone, F. Pentimalli, M. Fedele, R. Iuliano, M. Santoro, L. Chiariotti, A. Ballabio, and A. Fusco.** 2002. The homeodomain-interacting protein kinase 2 gene is expressed late in embryogenesis and preferentially in retina, muscle, and neural tissues. Biochem. Biophys. Res. Commun. **290:**942–947.
53. **Puri, P. L., K. Bhakta, L. D. Wood, A. Costanzo, J. Zhu, and J. Y. Wang.** 2002. A myogenic differentiation checkpoint activated by genotoxic stress. Nat. Genet. **32:**585–593.
54. **Rastegar, M., L. Kobrossy, E. N. Kovacs, I. Rambaldi, and M. Featherstone.** 2004. Sequential histone modifications at Hoxd4 regulatory regions distinguish anterior from posterior embryonic compartments. Mol. Cell. Biol. **24:**8090–8103.
55. **Rochat-Steiner, V., K. Becker, O. Micheau, P. Schneider, K. Burns, and J. Tschopp.** 2000. FIST/HIPK3: a Fas/FADD-interacting serine/threonine kinase that induces FADD phosphorylation and inhibits Fas-mediated Jun NH_2-terminal kinase activation. J. Exp. Med. **192:**1165–1174.
56. **Roelink, H., J. A. Porter, C. Chiang, Y. Tanabe, D. T. Chang, P. A. Beachy, and T. M. Jessell.** 1995. Floor plate and motor neuron induction by different concentrations of the amino-terminal cleavage product of Sonic hedgehog autoproteolysis. Cell **81:**445–455.
57. **Rui, Y., Z. Xu, S. Lin, Q. Li, H. Rui, W. Luo, H. M. Zhou, P. Y. Cheung, Z. Wu, Z. Ye, P. Li, J. Han, and S. C. Lin.** 2004. Axin stimulates p53 functions by activation of HIPK2 kinase through multimeric complex formation. EMBO J. **23:**4583–4594.
58. **Saga, Y., N. Hata, H. Koseki, and M. M. Taketo.** 1997. Mesp2: a novel mouse gene expressed in the presegmented mesoderm and essential for segmentation initiation. Genes Dev. **11:**1827–1839.
59. **Sah, V. P., L. D. Attardi, G. J. Mulligan, B. O. Williams, R. T. Bronson, and T. Jacks.** 1995. A subset of p53-deficient embryos exhibit exencephaly. Nat. Genet. **10:**175–180.
60. **Sung, K. S., Y. Y. Go, J. H. Ahn, Y. H. Kim, Y. Kim, and C. Y. Choi.** 2005. Differential interactions of the homeodomain-interacting protein kinase 2 (HIPK2) by phosphorylation-dependent sumoylation. FEBS Lett. **579:**3001–3008.
61. **Takebayashi-Suzuki, K., J. Funami, D. Tokumori, A. Saito, T. Watabe, K. Miyazono, A. Kanda, and A. Suzuki.** 2003. Interplay between the tumor suppressor p53 and TGF beta signaling shapes embryonic body axes in Xenopus. Development **130:**3929–3939.
62. **Wallin, J. W., H. Koseki, R. Fritsch, B. Christ, and R. Balling.** 1994. The role of *Pax1* in axial skeleton development. Development **120:**1109–1121.
63. **Wang, Y., E. M. Schneider, X. Li, I. Duttenhofer, K. Debatin, and H. Hug.** 2002. HIPK2 associates with RanBPM. Biochem. Biophys. Res. Commun. **297:**148–153.
64. **Watanabe, K., T. Ozaki, T. Nakagawa, K. Miyazaki, M. Takahashi, M. Hosoda, S. Hayashi, S. Todo, and A. Nakagawara.** 2002. Physical interaction of p73 with c-Myc and MM1, a c-Myc-binding protein, and modulation of the p73 function. J. Biol. Chem. **277:**15113–15123.
65. **Wiggins, A. K., G. Wei, E. Doxakis, C. Wong, A. A. Tang, K. Zang, E. J. Luo, R. L. Neve, L. F. Reichardt, and E. J. Huang.** 2004. Interaction of Brn3a and HIPK2 mediates transcriptional repression of sensory neuron survival. J. Cell Biol. **167:**257–267.
66. **Ybot-Gonzalez, P., P. Cogram, D. Gerrelli, and A. J. Copp.** 2002. Sonic hedgehog and the molecular regulation of mouse neural tube closure. Development **129:**2507–2517.
67. **Zakany, J., M. Kmita, P. Alarcon, J. L. de la Pompa, and D. Duboule.** 2001. Localized and transient transcription of Hox genes suggests a link between patterning and the segmentation clock. Cell **106:**207–217.
68. **Zhang, Q., Y. Yoshimatsu, J. Hildebrand, S. M. Frisch, and R. H. Goodman.** 2003. Homeodomain interacting protein kinase 2 promotes apoptosis by downregulating the transcriptional corepressor CtBP. Cell **115:**177–186.
69. **Zhang, Q., A. Nottke, and R. H. Goodman.** 2005. Homeodomain-interacting protein kinase-2 mediates CtBP phosphorylation and degradation in UV-triggered apoptosis. Proc. Natl. Acad. Sci. USA **102:**2802–2807.